AAS 23-067

LINEAR COVARIANCE TECHNIQUES TO ANALYZE A MULTI-VEHICLE, MULTI-GN&C SYSTEM WITH APPLICATIONS TO RENDEZVOUS IN A NEAR RECTILINEAR HALO ORBIT

David C. Woffinden*

Typically for a rendezvous and docking scenario, only a single vehicle is considered the active vehicle. As a result, the target vehicle's GN&C system is typically not a factor in the integrated performance analysis as it assumes a passive role. However, for upcoming NASA Artemis missions the active vehicle is both the chaser and target spacecraft. In addition, both vehicles are cooperating with one another, sharing telemetry data, and relying on data extracted from the GN&C system of the other. The process also includes a team of ground support personnel in mission control are tracking and monitoring each spacecraft uplinking state estimates and targeting solutions to support mission operations and enhance the onboard flight system performance. Being able to quickly analyze the impact of both vehicles with two different GN&C systems that also interact with the ground that does its own navigation and targeting uploads is critical. This paper outlines how to perform this rapid analysis using linear covariance techniques and applies them to a rendezvous scenario initiated in low lunar orbit and completed in a Near Rectilinear Halo Orbit (NRHO) representative of the NASA Artemis III mission.

INTRODUCTION

The crucial role and complexity associated with performing rendezvous, proximity operations, and docking (RPOD) was recognized from the initial development of major space flight programs. To simplify the inevitable intricacies associated with RPOD, one of the rendezvousing vehicles was designated as the target vehicle and essentially assumed a passive role allowing the critical activity to be performed by the assigned chaser vehicle. Although this paradigm is still adopted for many recent RPOD programs, as NASA extends its exploration initiatives to the Moon and beyond, both the chaser and target spacecraft are required to act as the active vehicle. Such is the case for the proposed Artemis III mission where Orion and a lunar lander developed by the Human Launch System (HLS) program must rendezvous together following the ascent of the lander from the lunar surface and re-rendezvous in an Earth-Moon Near Rectilinear Halo Orbit (NRHO) [1,2] as depicted in Figure 1. Orchestrating and analyzing this celestial waltz has necessitated new analytical techniques to provide quality yet rapid results.

This paper outlines linear covariance (LinCov) analysis techniques that accounts for multiple vehicles each having their own guidance, navigation, and control (GN&C) system. Rather than having the active chaser vehicle have the prominent role to carry out the RPOD operations, these new theoretical developments will accommodate and facilitate multiple GN&C systems in the LinCov framework. These general techniques can apply to GN&C performed onboard an orbiting spacecraft or similar operations enacted on the ground in a mission control setting. Although these concepts apply to any multi-vehicle, multi-GN&C system scenario, these core technical developments are motivated and given context with regards to a rendezvous scenario where a vehicle ascends from the lunar surface and eventually docks with another spacecraft in an NRHO replicating a NASA Artemis III mission.

*GN&C Autonomous Flight Systems Engineer, NASA JSC, Aeroscience and Flight Mechanics Division, david.c.woffinden@nasa.gov

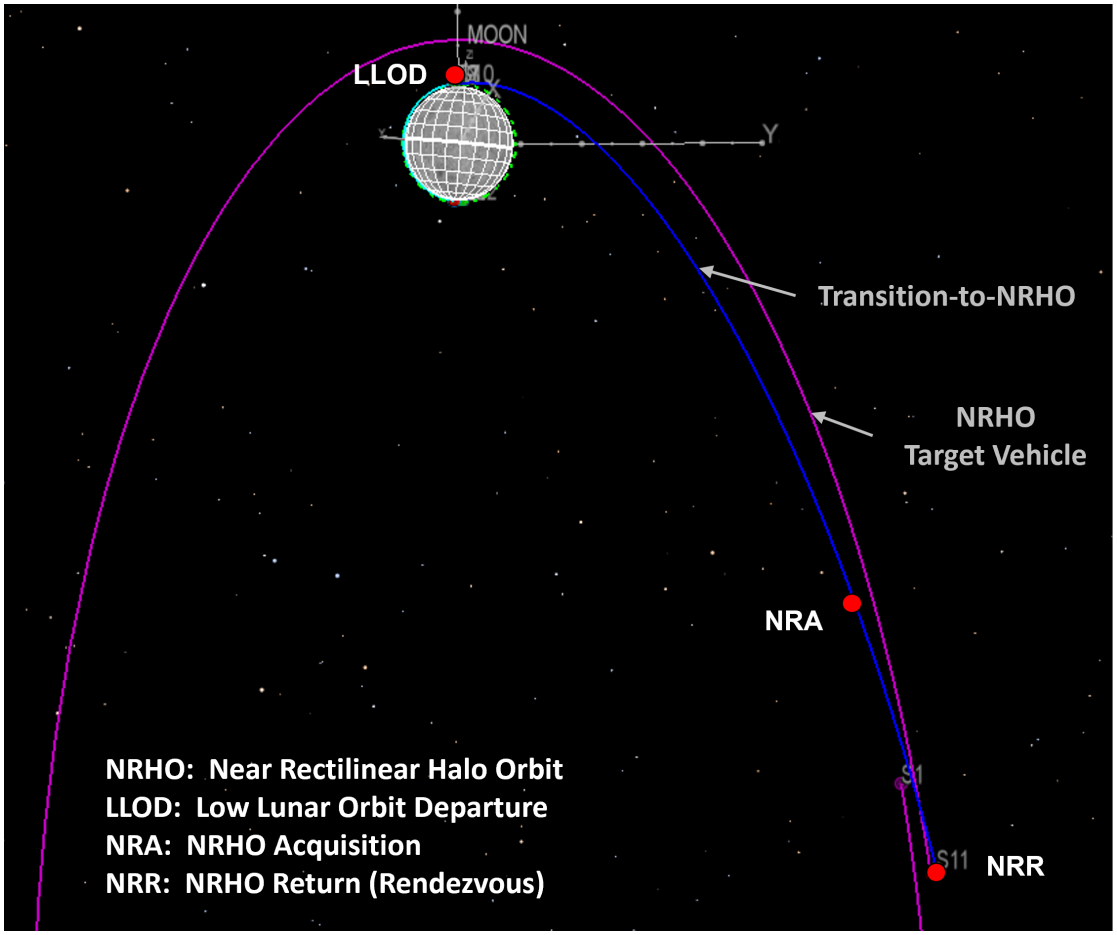

Figure 1. Notional Orion Artemis III Lunar Orbit to NRHO Rendezvous Transfer

Previous research efforts developed the linear covariance analysis techniques to model multiple sub-filters on a vehicle and evaluate an assortment of different types of filter formulations for a specific spacecraft [3]. Those developments assumed only a single vehicle with a navigation system that had multiple filters such as the Orion spacecraft that utilizes an Atmospheric EKF (ATMEKF), Attitude EKF (ATTEKF), Earth-Orbit EKF (EOEKF), and a Cis-lunar EKF (CLEKF) [4]. Each is active during a particular flight phase with some operating simultaneously to provide both the translational and rotational state estimates. The NASA Lunar Pallet Lander navigation architecture utilizes a similar navigation system where it has separate attitude and translational state filters [5]. The earlier LinCov developments highlighted how to represent these multiple filters running in parallel to provide a single state estimate for a navigation system of only one vehicle. The intent here is to extend the previous work by incorporating multiple vehicles (or ground stations) each with their own independently operating navigation filters and GN&C systems if applicable.

LINEAR COVARIANCE ANALYSIS PERFORMANCE METRICS

In order to develop the fundamental linear covariance formulation for a mission that entails a multi-vehicle, multi-GN&C system arrangement, there are several fundamental metrics that are produced to quantify the integrated performance. These performance metrics include the true trajectory dispersions $\delta\mathbf{x}$, the navigation dispersions $\delta\hat{\mathbf{x}}$, the true navigation error $\delta\mathbf{e}$, and the onboard navigation error $\delta\hat{\mathbf{e}}$ as depicted in Figure 2. The true dispersions $\delta\mathbf{x}$ are defined as the difference between the true state $\mathbf{x}$ and the nominal state $\bar{\mathbf{x}}$. The true

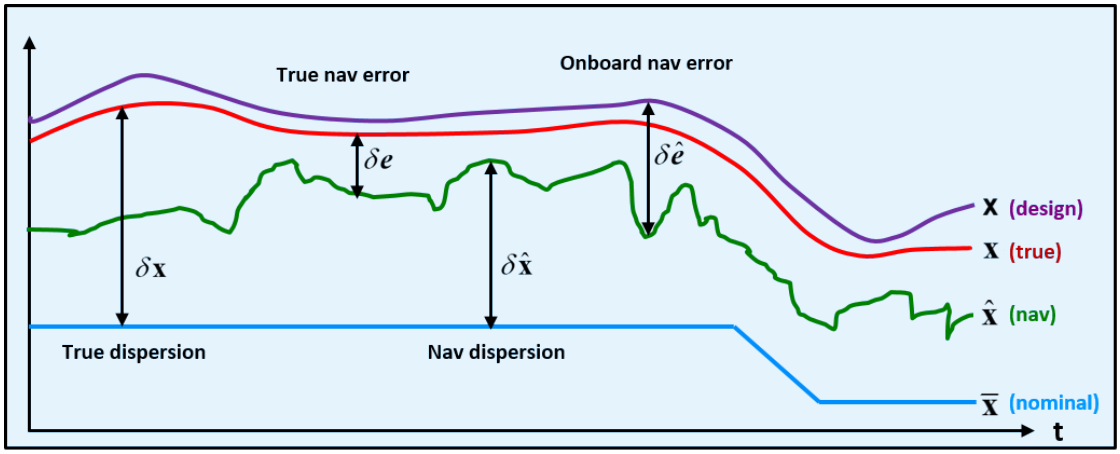

Figure 2. GN&C Performance Metric Variables

state $\mathbf{x}$ is an n-dimensional vector that represents the *real world* environment or actual state.

$$\delta \mathbf{x} \triangleq \mathbf{x} - \bar{\mathbf{x}} \qquad \mathbf{D} = E\left[\delta \mathbf{x} \delta \mathbf{x}^{\mathrm{T}}\right] \tag{1}$$

The nominal state $\bar{\mathbf{x}}$ is also an n-dimensional vector that represents the desired or reference state. The covariance of the environment dispersions, $\mathbf{D}$, indicates how precisely the system can follow a desired trajectory.

The navigation dispersions $\delta \hat{\mathbf{x}}$ are defined as the difference between the navigation state $\hat{\mathbf{x}}$ and the nominal state $\bar{\mathbf{x}}$. The navigation state is an $\hat{n}$-dimensional vector ($\hat{n} < n$) that represents the filter's estimated state.

$$\delta \hat{\mathbf{x}} \triangleq \hat{\mathbf{x}} - \hat{\mathbf{N}}_x \bar{\mathbf{x}} \qquad \hat{\mathbf{D}} = E\left[\delta \hat{\mathbf{x}} \delta \hat{\mathbf{x}}^{\mathrm{T}}\right] \tag{2}$$

The matrix $\hat{\mathbf{N}}_x$ is an $(\hat{n} \times n)$ matrix that maps the estimated state in terms of the true and nominal state. The covariance of the navigation dispersions, $\hat{\mathbf{D}}$, reflect how precisely the onboard system thinks it can follow a prescribed reference trajectory.

The true navigation error $\delta \mathbf{e}$ is the difference between the environment and navigation states. It is also the difference between the environment and the navigation dispersions.

$$\delta \mathbf{e} \triangleq \hat{\mathbf{N}}_x \mathbf{x} - \hat{\mathbf{x}} = \hat{\mathbf{N}}_x \delta \mathbf{x} - \delta \hat{\mathbf{x}} \qquad \mathbf{P} = E\left[\delta \mathbf{e} \delta \mathbf{e}^{\mathrm{T}}\right] \tag{3}$$

The covariance of the true navigation error, $\mathbf{P}$, quantifies how precisely the onboard navigation system can estimate the actual state.

The onboard navigation error $\delta \hat{\mathbf{e}}$ itself is never computed, but it is used to develop the onboard navigation filter equations. It is defined as the difference between the design state, x, and the navigation state $\hat{\mathbf{x}}$.

$$\delta \hat{\mathbf{e}} \triangleq \mathrm{x} - \hat{\mathbf{x}} \qquad \hat{\mathbf{P}} = E\left[\delta \hat{\mathbf{e}} \delta \hat{\mathbf{e}}^{\mathrm{T}}\right] \tag{4}$$

The covariance of the onboard navigation error, $\hat{\mathbf{P}}$, quantifies how precisely the onboard navigation system expects it can determine the actual state. The performance of the onboard navigation system is determined by comparing $\hat{\mathbf{P}}$ to the actual navigation performance $\mathbf{P}$. If the *true* states and the *design* states are assumed to be the same, then the true navigation covariance will equal the onboard navigation covariance.

The covariances of the true dispersions, navigation dispersions, true navigation error, and the onboard navigation error are ultimately used to analyze and assess the performance of a proposed GN&C system. A common approach to obtain these performance metrics is to use a Monte Carlo simulation outlined in Figure

3, where the sample statistics of hundreds or thousands of runs, N, are used to numerically compute the desired covariance matrices.

$$\mathbf{D} = \frac{1}{N-1}\sum \delta\mathbf{x}\delta\mathbf{x}^{\mathrm{T}} \qquad \hat{\mathbf{D}} = \frac{1}{N-1}\sum \delta\hat{\mathbf{x}}\delta\hat{\mathbf{x}}^{\mathrm{T}} \qquad \mathbf{P} = \frac{1}{N-1}\sum \delta\mathbf{e}\delta\mathbf{e}^{\mathrm{T}} \tag{5}$$

The onboard navigation error covariance $\hat{\mathbf{P}}$ is the navigation filter covariance for each run. This same statistical information can be obtained using linear covariance analysis techniques.

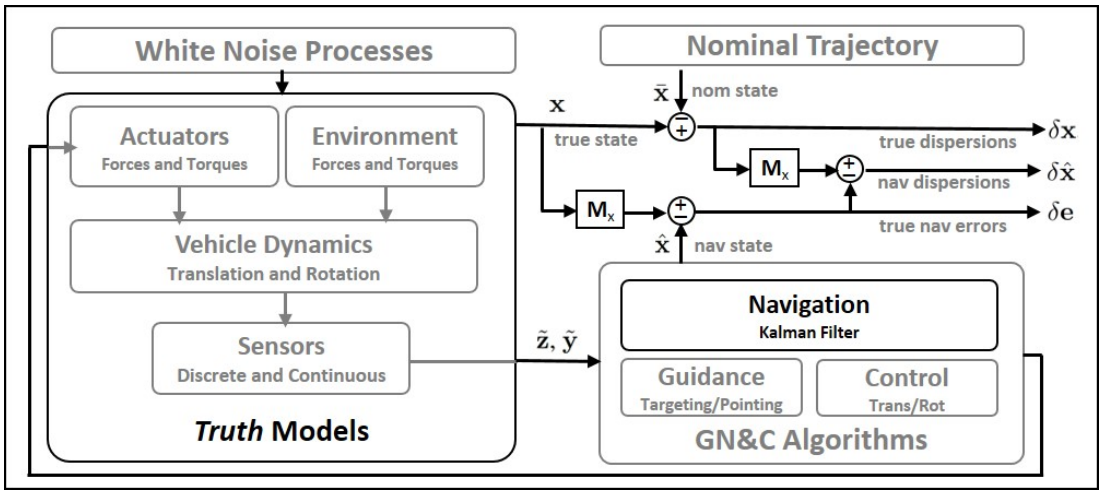

Figure 3. Extracting GN&C Performance Metrics Using Monte Carlo Techniques

Linear covariance analysis incorporates the non-linear system dynamics models and GN&C algorithms to generate a nominal reference trajectory $\bar{\mathbf{x}}$ which is then used to propagate, update, and correct an onboard navigation covariance matrix $\hat{\mathbf{P}}$ and an augmented state covariance matrix $\mathbf{C}$,

$$\mathbf{C} = E\left[\delta\mathbf{X}\delta\mathbf{X}^{\mathrm{T}}\right] \tag{6}$$

where the augmented state $\delta\mathbf{X}^{\mathrm{T}} = [\delta\mathbf{x}^{\mathrm{T}}\ \delta\hat{\mathbf{x}}^{\mathrm{T}}]$ consists of the true dispersions and the navigation dispersions. Pre- and post-multiplying the augmented state covariance matrix by the following mapping matrices, the covariances for the trajectory dispersions, navigation dispersions, and the navigation error can be obtained.

$$\begin{aligned}
\mathbf{D} &= [\,\mathbf{I}_{n\times n},\ \mathbf{0}_{n\times\hat{n}}\,]\,\mathbf{C}\,[\,\mathbf{I}_{n\times n},\ \mathbf{0}_{n\times\hat{n}}\,]^{\mathrm{T}} \\
\hat{\mathbf{D}} &= [\,\mathbf{0}_{\hat{n}\times n},\ \mathbf{I}_{\hat{n}\times\hat{n}}\,]\,\mathbf{C}\,[\,\mathbf{0}_{\hat{n}\times n},\ \mathbf{I}_{\hat{n}\times\hat{n}}\,]^{\mathrm{T}} \\
\mathbf{P} &= \left[\,\hat{\mathbf{N}}_x,\ -\mathbf{I}_{\hat{n}\times\hat{n}}\,\right]\mathbf{C}\left[\,\hat{\mathbf{N}}_x,\ -\mathbf{I}_{\hat{n}\times\hat{n}}\,\right]^{\mathrm{T}}
\end{aligned} \tag{7}$$

For additional details regarding the development and implementation of the linear covariance simulation, see the following references [6–11].

MULTI-VEHICLE, MULTI-GN&C SYSTEM MODELING

For RPOD analysis where multiple vehicles operate simultaneously, typically the dynamics of two vehicles are captured, the chaser and target vehicles. The target vehicle is assumed to be passive and the chaser vehicle active, such that only the chaser vehicle's GN&C system is modeled. This assumed operational mode for analysis purposes is depicted in Figure 4(a). Typically the target vehicle sensors and GN&C algorithms are ignored since the basic assumption is that the target vehicle does not do any translational burns (and the attitude profile holds a predetermined orientation). This section derives the fundamental linear covariance

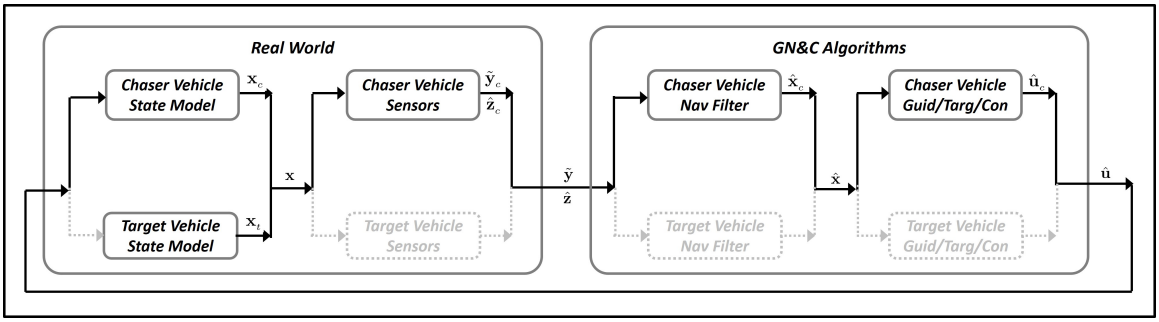

(a) Typical RPOD GN&C Architecture

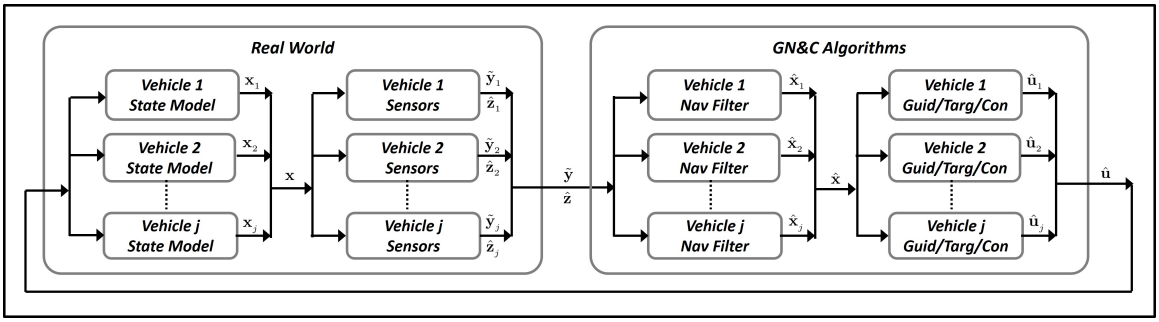

(b) General Multi-Vehicle, Multi-GN&C Architecture

Figure 4. GN&C Architectures for RPOD

equations to support an arbitrary number of vehicles and GN&C systems, each having independently operating navigation filters. This multi-vehicle, multi-GN&C system architecture is highlighted in Figure 4(b). Although the mathematical derivation will be generic and applicable for a variety of phases of space flight, context and motivation will be provided through the lens of rendezvous and docking.

LinCov States for Multi-Vehicle, Multi-GN&C Systems

The n-dimensional true state vector $\mathbf{x}$ defined previously, now consists of all the states for j-vehicles; $\mathbf{x}_1$, $\mathbf{x}_2$, ... $\mathbf{x}_j$ where any additional states due to atmosphere or other general environmental parameters are not emphasized in this derivation.

$$\mathbf{x} = [\mathbf{x}_1;\ \mathbf{x}_2;\ ...;\ \mathbf{x}_j] \tag{8}$$

Generally each vehicle state consists of the vehicle's core states $\mathbf{x}_v$ such as inertial position, inertial velocity, attitude, and angular rates; and the vehicle's parameter states $\mathbf{x}_p$ which may include any sensor, actuator, or performance states [10].

$$\mathbf{x}_j = [\mathbf{x}_{v_j};\ \mathbf{x}_{p_j}] \tag{9}$$

The navigation state $\hat{\mathbf{x}}$ now consists of each state corresponding to each vehicle's navigation filter $\hat{\mathbf{x}}_j$,

$$\hat{\mathbf{x}} = [\hat{\mathbf{x}}_1;\ \hat{\mathbf{x}}_2;\ ...;\ \hat{\mathbf{x}}_j] \tag{10}$$

where each filter can potentially estimate each truth state. This implies the navigation filter on j-vehicle can have a dimension equal to or less than the number of true states, $\hat{n}_j \leq n$. For example, the navigation filter for Vehicle #1 can include the state estimate of itself $\hat{\mathbf{x}}_{11}$, the second vehicle $\hat{\mathbf{x}}_{12}$, up to the j^{th} vehicle states $\hat{\mathbf{x}}_{1j}$ where the first sub-number represents the current filter and the second captures which vehicle state it represents. If each vehicle's filter adopted a similar assumption, then the navigation state $\hat{\mathbf{x}}$ could include the following,

$$\hat{\mathbf{x}}_1 = [\hat{\mathbf{x}}_{11};\ \hat{\mathbf{x}}_{12};\ ...\ \hat{\mathbf{x}}_{1j}], \quad \hat{\mathbf{x}}_2 = [\hat{\mathbf{x}}_{21};\ \hat{\mathbf{x}}_{22};\ ...\ \hat{\mathbf{x}}_{2j}], \quad \ldots, \quad \hat{\mathbf{x}}_j = [\hat{\mathbf{x}}_{j1};\ \hat{\mathbf{x}}_{j2};\ ...\ \hat{\mathbf{x}}_{jj}]$$

This implies the $\hat{n}$-dimensional navigation state $\hat{\mathbf{x}}$ can now be as large as j-times the number of truth states once the inclusion of each vehicle's filter is included.

$$\hat{n} \leq (j \times n) \tag{11}$$

However, it is likely that each vehicle will not try to estimate the parameter states of the other vehicles such as sensor biases or thruster misalignments. Instead, they will likely include only the core states such as inertial position, velocity and possibly attitude and angular rates so that the total number of navigation states does not reach the potential limit. Given the mapping-matrix of each vehicle's filter state $\mathbf{M}_j$ from the truth state,

$$\hat{\mathbf{x}}_1 = \mathbf{M}_1\mathbf{x}, \qquad \hat{\mathbf{x}}_2 = \mathbf{M}_2\mathbf{x}, \qquad \ldots, \qquad \hat{\mathbf{x}}_j = \mathbf{M}_j\mathbf{x}$$

the general navigation mapping matrix $\mathbf{M}_x$ introduced previously to show how the true states and navigation states are defined $\hat{\mathbf{x}} = \mathbf{M}_x\mathbf{x}$, now accounts for each filter on each vehicle.

$$\mathbf{M}_x = [\mathbf{M}_1;\ \mathbf{M}_2; \ldots ;\ \mathbf{M}_j] \tag{12}$$

This implies the navigation dispersions $\delta\hat{\mathbf{x}}$ in Eqn 2, the true navigation error $\delta\mathbf{e}$ in Eqn 3 and the onboard navigation error $\delta\hat{\mathbf{e}}$ in Eqn 4 can be expressed as a function of each vehicle's navigation filter states,

$$\delta\hat{\mathbf{x}} = [\delta\hat{\mathbf{x}}_1, \delta\hat{\mathbf{x}}_2, ..., \delta\hat{\mathbf{x}}_j], \qquad \delta\mathbf{e} = [\delta\mathbf{e}_1, \delta\mathbf{e}_2, ..., \delta\mathbf{e}_j], \qquad \delta\hat{\mathbf{e}} = [\delta\hat{\mathbf{e}}_1, \delta\hat{\mathbf{e}}_2, ..., \delta\hat{\mathbf{e}}_j] \tag{13}$$

LinCov Modeling for Multi-Vehicle, Multi-GN&C System

Now that the additional LinCov states have been identified, this section introduces the mathematical formulation behind modeling a multi-vehicle, multi-GN&C system in LinCov. The fundamental equations associated with initializing propagating, updating, and correcting both the onboard navigation covariance matrix $\hat{\mathbf{P}}$ and the augmented state covariance matrix $\mathbf{C}$ are derived.

A basic premise behind an architecture that has multiple vehicles and consequently the potential of a variety of different navigation filters, whether on the ground for mission operations or onboard the spacecraft as part of the vehicle's flight software, is that they operate independently of one another. This does not mean data, measurements, or even states cannot be shared among each other, it implies each filter operates independent of the others. Consequently, the basic premise for a multi-vehicle filter formulation is that the true and onboard navigation errors associated with a particular vehicle filter are independent from the states utilized in the other filters such that the correlation terms between filters are zero

$$E[\delta\mathbf{e}_i\delta\mathbf{e}_j^T] = \mathbf{0} \qquad E[\delta\hat{\mathbf{e}}_i\delta\hat{\mathbf{e}}_j^T] = \mathbf{0} \qquad \text{for } i \neq j \tag{14}$$

For example, the onboard state covariance matrix $\hat{\mathbf{P}}$ equals

$$\hat{\mathbf{P}} = E[\delta\hat{\mathbf{e}}\delta\hat{\mathbf{e}}^T] = \begin{bmatrix} E[\delta\hat{\mathbf{e}}_1\delta\hat{\mathbf{e}}_1^T] & E[\delta\hat{\mathbf{e}}_1\delta\hat{\mathbf{e}}_2^T] & ... & E[\delta\hat{\mathbf{e}}_1\delta\hat{\mathbf{e}}_j^T] \\ E[\delta\hat{\mathbf{e}}_2\delta\hat{\mathbf{e}}_1^T] & E[\delta\hat{\mathbf{e}}_2\delta\hat{\mathbf{e}}_2^T] & ... & E[\delta\hat{\mathbf{e}}_2\delta\hat{\mathbf{e}}_j^T] \\ \vdots & \vdots & \ddots & \vdots \\ E[\delta\hat{\mathbf{e}}_j\delta\hat{\mathbf{e}}_1^T] & E[\delta\hat{\mathbf{e}}_m\delta\hat{\mathbf{e}}_2^T] & ... & E[\delta\hat{\mathbf{e}}_j\delta\hat{\mathbf{e}}_j^T] \end{bmatrix} \tag{15}$$

Substituting assumptions in Eqn 14, the only alteration to the onboard navigation covariance matrix is nulling out the cross-correlation terms between the different vehicle filter states, $[\hat{\mathbf{P}}\diagdown] = \mathbf{0}$.

$$\hat{\mathbf{P}} = \begin{bmatrix} \hat{\mathbf{P}}_1 & \mathbf{0} & ... & \mathbf{0} \\ \mathbf{0} & \hat{\mathbf{P}}_2 & ... & \mathbf{0} \\ \vdots & \vdots & \ddots & \vdots \\ \mathbf{0} & \mathbf{0} & ... & \hat{\mathbf{P}}_j \end{bmatrix} \tag{16}$$

For the augmented state covariance matrix, it too must be modified to properly mimic multiple vehicle-filters. Utilizing the navigation dispersions $\delta\hat{\mathbf{x}}$ outlined in Eqn 13, the augmented state becomes $\delta\mathbf{X} = [\delta\mathbf{x};\ \delta\hat{\mathbf{x}}]$, such that

$$\mathbf{C} = E[\delta\mathbf{X}\ \delta\mathbf{X}^T] = \begin{bmatrix} E[\delta\mathbf{x}\ \delta\mathbf{x}^{\mathrm{T}}] & E[\delta\mathbf{x}\ \delta\hat{\mathbf{x}}^T] \\ E[\delta\hat{\mathbf{x}}\ \delta\mathbf{x}] & E[\delta\hat{\mathbf{x}}\ \delta\hat{\mathbf{x}}^T] \end{bmatrix} = \begin{bmatrix} \mathbf{D} & \bar{\mathbf{D}} \\ \bar{\mathbf{D}}^T & \hat{\mathbf{D}} \end{bmatrix} \tag{17}$$

Note that the cross correlation term between the true dispersions $\delta\mathbf{x}$ and the vehicle-filter navigation dispersions $\delta\hat{\mathbf{x}}$ are not constrained to be zero such that $E[\delta\mathbf{x}\ \delta\hat{\mathbf{x}}^T] = E[\delta\mathbf{x}\ \delta\hat{\mathbf{x}}^T] = \bar{\mathbf{D}}$. As a result, the augmented state covariance matrix $\mathbf{C}$ consists of the true dispersions $\mathbf{D}$, the navigation dispersions $\hat{\mathbf{D}}$, and the cross correlation matrix $\bar{\boldsymbol{D}}$.

The question remaining is what value should the matrix $\hat{\mathbf{D}}$ be in order to ensure the correlation between the true navigation error of each vehicle-filter remains independent and consequently zero? Recall that the true navigation error covariance matrix $\mathbf{P}$ can be derived from the augmented state covariance matrix $\mathbf{C}$ as defined in Eqn 7.

$$\mathbf{P} = \begin{bmatrix} \hat{\mathbf{N}}_x,\ -\hat{\mathbf{I}} \end{bmatrix} \mathbf{C} \begin{bmatrix} \hat{\mathbf{N}}_x,\ -\hat{\mathbf{I}} \end{bmatrix}^{\mathrm{T}} \tag{18}$$

Substituting Eqn 17 into Eqn 18 yields the following expression for the true navigation error covariance matrix

$$\mathbf{P} = \hat{\mathbf{D}} + \hat{\mathbf{N}}_x\mathbf{D}\hat{\mathbf{N}}_x^{\mathrm{T}} - \hat{\mathbf{N}}_x\bar{\mathbf{D}} - \bar{\mathbf{D}}^T\hat{\mathbf{N}}_x^{\mathrm{T}} \tag{19}$$

Now, the off-diagonal terms of $\mathbf{P}$ must be zero to ensure the filters are independent of one another such that $[\mathbf{P}\diagdown] = \mathbf{0}$. Substituting the expression for $\mathbf{P}$ in Eqn 19 gives,

$$\mathbf{0} = \left[\left(\hat{\mathbf{D}} + \hat{\mathbf{N}}_x\mathbf{D}\hat{\mathbf{N}}_x^{\mathrm{T}} - \hat{\mathbf{N}}_x\bar{\mathbf{D}} - \bar{\mathbf{D}}^T\hat{\mathbf{N}}_x^{\mathrm{T}} \right) \diagdown \right] \tag{20}$$

This can be accomplished if the off-diagonal terms of $\hat{\mathbf{D}}$ equal the off-diagonal terms of the following,

$$\left[\hat{\mathbf{D}} \diagdown \right] = \left[\left(\hat{\mathbf{N}}_x\bar{\mathbf{D}} + \bar{\mathbf{D}}^T\hat{\mathbf{N}}_x^{\mathrm{T}} - \hat{\mathbf{N}}_x\mathbf{D}\hat{\mathbf{N}}_x^{\mathrm{T}} \right) \diagdown \right] \tag{21}$$

In summary, the only modification to the augmented state covariance matrix $\mathbf{C}$ to ensure the navigation errors between the states associated with the different vehicle filters are uncorrelated is achieved by ensuring the off-diagonal terms of the navigation dispersion covariance matrix $\hat{\mathbf{D}}$ equal the quantity derived in Eqn 21.

Initialization To initialize the augmented state consisting of multiple vehicle states with a specific initial dispersions $\delta\mathbf{x}_0$ and navigation error $\delta\hat{\mathbf{e}}_0$ with covariances $\mathbf{D}_0$ and $\hat{\mathbf{P}}_0$ respectively that captures each spacecraft,

$$\mathbf{D}_0 = E\left[\delta\mathbf{x}_0\ \delta\mathbf{x}_0^{\mathrm{T}}\right] \tag{22}$$

$$\hat{\mathbf{P}}_0 = E\left[\delta\hat{\mathbf{e}}_0\ \delta\hat{\mathbf{e}}_0^{\mathrm{T}}\right] \tag{23}$$

recall from Eqn 3 that the initial navigation error is defined as the difference between the true and navigation initial dispersions.

$$\delta\mathbf{e}_0 = \hat{\mathbf{N}}_x\delta\mathbf{x}_0 - \delta\hat{\mathbf{x}}_0. \tag{24}$$

By setting the initial navigation dispersions to reflect the initial onboard navigation error $\delta\hat{\mathbf{x}}_0 = \hat{\mathbf{N}}_x\delta\mathbf{x}_0 - \delta\hat{\mathbf{e}}_0$, the initial augmented state, $\delta\mathbf{X}_0$ can be set to incorporate both a particular initial trajectory dispersion and navigation error,

$$\delta\mathbf{X}_0 = \begin{bmatrix} \delta\mathbf{x}_0 \\ \left(\hat{\mathbf{N}}_x\delta\mathbf{x}_0 - \delta\hat{\mathbf{e}}_0 \right) \end{bmatrix} \tag{25}$$

Consequently, the initial augmented state covariance, $\mathbf{C}_0$, from Eqn 6 becomes,

$$\mathbf{C}_0 = \begin{bmatrix} E\left[\delta\mathbf{x}_0\ \delta\mathbf{x}_0^{\mathrm{T}}\right] & E\left[\delta\mathbf{x}_0\ \delta\mathbf{x}_0^{\mathrm{T}}\right]\hat{\mathbf{N}}_x^{\mathrm{T}} \\ \hat{\mathbf{N}}_x E\left[\delta\mathbf{x}_0\ \delta\mathbf{x}_0^{\mathrm{T}}\right] & \hat{\mathbf{N}}_x E\left[\delta\mathbf{x}_0\ \delta\mathbf{x}_0^{\mathrm{T}}\right]\hat{\mathbf{N}}_x^{\mathrm{T}} + E\left[\delta\hat{\mathbf{e}}_0\ \delta\hat{\mathbf{e}}_0^{\mathrm{T}}\right] \end{bmatrix} \tag{26}$$

when the initial trajectory dispersions and navigation error are assumed to be independent $E\left[\delta\hat{\mathbf{x}}_0\ \delta\bar{\mathbf{e}}_0^{\mathrm{T}}\right] = \mathbf{0}$. By substituting the definition of the initial dispersion $\mathbf{D}_0$ and navigation error covariance matrices $\hat{\mathbf{P}}_0$ from Eqn 22 and 23 respectively into Eqn 26, the initial augmented state covariance matrix in terms of the initial onboard state covariance matrix is

$$\mathbf{C}_0 = \begin{bmatrix} \mathbf{D}_0 & \mathbf{D}_0\hat{\mathbf{N}}_x^{\mathrm{T}} \\ \hat{\mathbf{N}}_x\mathbf{D}_0 & \hat{\mathbf{N}}_x\mathbf{D}_0\hat{\mathbf{N}}_x^{\mathrm{T}} + \hat{\mathbf{P}}_0 \end{bmatrix} \tag{27}$$

The initial true dispersion covariance matrix $\mathbf{D}_0$ for a multi-vehicle system can be initialized either assuming correlation between vehicles or without correlations. The correlation terms allow the relative dispersions between vehicles to be defined, which can be a vital capability for rendezvous and proximity operations. For example, the initial true state dispersions matrix $\mathbf{D}_0$ equals

$$\mathbf{D}_0 = E[\delta\mathbf{x}_0\delta\mathbf{x}_0^T] = \begin{bmatrix} E[\delta\mathbf{x}_{0_1}\delta\mathbf{x}_{0_1}^T] & E[\delta\mathbf{x}_1\delta\mathbf{x}_2^T] & ... & E[\delta\mathbf{x}_1\delta\mathbf{x}_j^T] \\ E[\delta\mathbf{x}_2\delta\mathbf{x}_1^T] & E[\delta\mathbf{x}_2\delta\mathbf{x}_2^T] & ... & E[\delta\mathbf{x}_2\delta\mathbf{x}_j^T] \\ \vdots & \vdots & \ddots & \vdots \\ E[\delta\mathbf{x}_j\delta\mathbf{x}_1^T] & E[\delta\mathbf{x}_j\delta\mathbf{x}_2^T] & ... & E[\delta\mathbf{x}_j\delta\mathbf{x}_j^T] \end{bmatrix} = \begin{bmatrix} \mathbf{D}_{0_{11}} & \mathbf{D}_{0_{12}} & ... & \mathbf{D}_{0_{1j}} \\ \mathbf{D}_{0_{21}} & \mathbf{D}_{0_{22}} & ... & \mathbf{D}_{0_{2j}} \\ \vdots & \vdots & \ddots & \vdots \\ \mathbf{D}_{0_{j1}} & \mathbf{D}_{0_{j2}} & ... & \mathbf{D}_{0_{jj}} \end{bmatrix} \tag{28}$$

For cases where the initial separation distance between the vehicles is large and the relative dispersions are largely unknown and not a key driver, then an reasonable approach for initializing the trajectory dispersions is merely nulling out the cross-correlation terms between the different vehicle states, $\mathbf{D}_{0_{ij}} = 0$.

$$\mathbf{D}_0 = \begin{bmatrix} \mathbf{D}_{0_{11}} & \mathbf{0} & ... & \mathbf{0} \\ \mathbf{0} & \mathbf{D}_{0_{22}} & ... & \mathbf{0} \\ \vdots & \vdots & \ddots & \vdots \\ \mathbf{0} & \mathbf{0} & ... & \mathbf{D}_{0_{jj}} \end{bmatrix} \tag{29}$$

For situations where defining the relative dispersions between two vehicles is important, then the cross correlations can be strategically set such that they are non-zero $\mathbf{D}_{0_{ij}} \neq 0$. For the initial navigation error $\hat{\mathbf{P}}_0$, the correlation terms between filters must be zero $\hat{\mathbf{P}}_{0_{ij}} = 0$ as outlined previously.

$$\hat{\mathbf{P}}_0 = \begin{bmatrix} \hat{\mathbf{P}}_{0_{11}} & \mathbf{0} & ... & \mathbf{0} \\ \mathbf{0} & \hat{\mathbf{P}}_{0_{22}} & ... & \mathbf{0} \\ \vdots & \vdots & \ddots & \vdots \\ \mathbf{0} & \mathbf{0} & ... & \hat{\mathbf{P}}_{0_{jj}} \end{bmatrix} \tag{30}$$

However, each vehicle can initialize its filter $\hat{\mathbf{P}}_{0_{jj}}$ such that both inertial as well as relative navigation errors between any vehicle can be specified, for that specific vehicle and filter implementation.

Propagation The continuous-time propagation equations for the augmented state covariance matrix $\mathbf{C}$ and the onboard navigation covariance matrix $\hat{\mathbf{P}}$ for non-continuous thrust applications are

$$\dot{\mathbf{C}} = \mathbf{F}\mathbf{C} + \mathbf{C}\mathbf{F}^T + \mathbf{W}\mathbf{S}_w\mathbf{W}^T \tag{31}$$

$$\dot{\hat{\mathbf{P}}} = \hat{\mathbf{F}}\hat{\mathbf{P}} + \hat{\mathbf{P}}\hat{\mathbf{F}}^T + \hat{\mathbf{W}}\hat{\mathbf{S}}_w\hat{\mathbf{W}}^T \tag{32}$$

where $\mathbf{F}$ and $\hat{\mathbf{F}}$ are augmented and onboard state Jacobians respectively for the linearized perturbation dynamics about the reference trajectory. The mapping matrices, $\mathbf{W}$ and $\hat{\mathbf{W}}$, are used to map environmental and navigation process noise such as gravity perturbations characterized by $\mathbf{S}_w$ and $\hat{\mathbf{S}}_w$, into $\mathbf{C}$ and $\hat{\mathbf{P}}$.

Update The measurement update equations for augmented and navigation state covariance matrices, $\mathbf{C}$ and $\hat{\mathbf{P}}$, are developed in this section. The potential discrete sensor measurements $\tilde{\mathbf{z}}$ utilized on each vehicle can be numerous. Given a multi-vehicle, mult-GN&C arrangement, incorporating these assortment of measurements on each spacecraft increases the complexity so a more detailed discussion is provided for this phase of the LinCov formulation.

Measurements provide information to support the estimation of the a vehicle's filter states, but measurements themselves do not alter the actual physical state of any spacecraft. As a result, the true state after a measurement update $\mathbf{x}^+$ equals the true state prior to the measurement update $\mathbf{x}^-$. However, the navigation state after a measurement update $\hat{\mathbf{x}}^+$ is altered from its value prior to the measurement $\hat{\mathbf{x}}^-$ based on the difference between the actual measurement $\tilde{\mathbf{z}}$ and the predicted measurement $\hat{\mathbf{z}}$,

$$\left.\begin{array}{l} \mathbf{x}_1^+ = \mathbf{x}_1^- \\ \mathbf{x}_2^+ = \mathbf{x}_2^- \\ \vdots \\ \mathbf{x}_j^+ = \mathbf{x}_j^- \end{array}\right\} \mathbf{x}^+ = \mathbf{x}^- \qquad \left.\begin{array}{l} \hat{\mathbf{x}}_1^+ = \hat{\mathbf{x}}_1^- + \hat{\mathbf{K}}_1 \left[\tilde{\mathbf{z}}_1 - \hat{\mathbf{z}}_1\right] \\ \hat{\mathbf{x}}_2^+ = \hat{\mathbf{x}}_2^- + \hat{\mathbf{K}}_2 \left[\tilde{\mathbf{z}}_2 - \hat{\mathbf{z}}_2\right] \\ \vdots \\ \hat{\mathbf{x}}_j^+ = \hat{\mathbf{x}}_j^- + \hat{\mathbf{K}}_j \left[\tilde{\mathbf{z}}_j - \hat{\mathbf{z}}_j\right] \end{array}\right\} \hat{\mathbf{x}}^+ = \hat{\mathbf{x}}^- + \hat{\mathbf{K}}\left[\tilde{\mathbf{z}} - \hat{\mathbf{z}}\right] \tag{33}$$

where $\hat{\mathbf{K}}_1$, $\hat{\mathbf{K}}_2$, and $\hat{\mathbf{K}}_j$ are the Kalman gains for the navigation filters on the first vehicle, second vehicle, and j-vehicle respectively, such that $\hat{\mathbf{K}}$ equals

$$\left.\begin{array}{l} \hat{\mathbf{K}}_1 = \hat{\mathbf{P}}_1^- \hat{\mathbf{H}}_1^T \left[\hat{\mathbf{H}}_1 \hat{\mathbf{P}}_1^- \hat{\mathbf{H}}_1^T + \hat{\mathbf{R}}_1\right]^{-1} \\ \hat{\mathbf{K}}_2 = \hat{\mathbf{P}}_2^- \hat{\mathbf{H}}_1^T \left[\hat{\mathbf{H}}_2 \hat{\mathbf{P}}_2^- \hat{\mathbf{H}}_2^T + \hat{\mathbf{R}}_2\right]^{-1} \\ \vdots \\ \hat{\mathbf{K}}_j = \hat{\mathbf{P}}_j^- \hat{\mathbf{H}}_j^T \left[\hat{\mathbf{H}}_j \hat{\mathbf{P}}_j^- \hat{\mathbf{H}}_j^T + \hat{\mathbf{R}}_j\right]^{-1} \end{array}\right\} \hat{\mathbf{K}} = \begin{bmatrix} \hat{\mathbf{K}}_1 & \mathbf{0} & \ldots & \mathbf{0} \\ \mathbf{0} & \hat{\mathbf{K}}_2 & \ldots & \mathbf{0} \\ \vdots & \vdots & \ddots & \vdots \\ \mathbf{0} & \mathbf{0} & \ldots & \hat{\mathbf{K}}_j \end{bmatrix} \tag{34}$$

The true measurement for a particular vehicle $\tilde{\mathbf{z}}_j$ is a function of the true state $\mathbf{x}^-$ and the actual measurement noise $\boldsymbol{\epsilon}_j$ associated with the vehicle's selected sensors suite. The strength of the discrete measurement noise is $E\left[\boldsymbol{\epsilon}_{j_k} \boldsymbol{\epsilon}_{j_{k'}}^T\right] = \mathbf{R}_j \; \delta_{kk'}$. A vehicle's predicted measurement $\hat{\mathbf{z}}_j$ is a function of that vehicle's filter navigation states just prior to the measurement update $\hat{\mathbf{x}}_j^-$. The anticipated sensor noise $\hat{\boldsymbol{\epsilon}}_j$ assumed onboard the spacecraft has the following covariance, $E\left[\hat{\boldsymbol{\epsilon}}_{j_k} \hat{\boldsymbol{\epsilon}}_{j_{k'}}^T\right] = \hat{\mathbf{R}}_j \; \delta_{kk'}$

$$\left.\begin{array}{l} \tilde{\mathbf{z}}_1 = \mathbf{h}_1(\mathbf{x}^-, \boldsymbol{\epsilon}_1) \\ \tilde{\mathbf{z}}_2 = \mathbf{h}_2(\mathbf{x}^-, \boldsymbol{\epsilon}_2) \\ \vdots \\ \tilde{\mathbf{z}}_j = \mathbf{h}_j(\mathbf{x}^-, \boldsymbol{\epsilon}_j) \end{array}\right\} \tilde{\mathbf{z}} = \mathbf{h}(\mathbf{x}^-, \boldsymbol{\epsilon}) \qquad \left.\begin{array}{l} \hat{\mathbf{z}}_1 = \hat{\mathbf{h}}_1(\hat{\mathbf{x}}_1^-) \\ \hat{\mathbf{z}}_2 = \hat{\mathbf{h}}_2(\hat{\mathbf{x}}_2^-) \\ \vdots \\ \hat{\mathbf{z}}_j = \hat{\mathbf{h}}_j(\hat{\mathbf{x}}_j^-) \end{array}\right\} \hat{\mathbf{z}} = \hat{\mathbf{h}}(\hat{\mathbf{x}}^-) \tag{35}$$

The update equations in Eqn 33 and Eqn 35 are linearized to produce the measurement update for both the true state dispersions $\delta\mathbf{x}^+$, the navigation dispersions $\delta\hat{\mathbf{x}}^+$, and the onboard navigation error $\delta\hat{\mathbf{e}}^+$

$$\delta\mathbf{x}^+ = \delta\mathbf{x}^- \qquad \delta\hat{\mathbf{x}}^+ = \left[\hat{\mathbf{K}}\mathbf{H}_x\right]\delta\mathbf{x}^- + \left[\mathbf{I} - \hat{\mathbf{K}}\hat{\mathbf{H}}\right]\delta\hat{\mathbf{x}}^- + \hat{\mathbf{K}}\boldsymbol{\epsilon} \qquad \delta\hat{\mathbf{e}}^+ = \left[\mathbf{I} - \hat{\mathbf{K}}\hat{\mathbf{H}}\right]\delta\hat{\mathbf{e}}^- - \hat{\mathbf{K}}\hat{\boldsymbol{\epsilon}} \tag{36}$$

where the partial of the true measurement with respect to the true state $\mathbf{H}_\mathbf{x}$, and the partial of the estimated measurement with respect to the estimated state $\hat{\mathbf{H}}$ are

$$\left.\begin{array}{l} \mathbf{H}_1 = \left.\frac{\partial \mathbf{h}_1(\mathbf{x}, \boldsymbol{\epsilon}_1)}{\partial \mathbf{x}}\right|_{\bar{\mathbf{x}}} \\ \mathbf{H}_2 = \left.\frac{\partial \mathbf{h}_2(\mathbf{x}, \boldsymbol{\epsilon}_2)}{\partial \mathbf{x}}\right|_{\bar{\mathbf{x}}} \\ \vdots \\ \mathbf{H}_j = \left.\frac{\partial \mathbf{h}_j(\mathbf{x}, \boldsymbol{\epsilon}_j)}{\partial \mathbf{x}}\right|_{\bar{\mathbf{x}}} \end{array}\right\} \mathbf{H}_\mathbf{x} = \left.\frac{\partial \mathbf{h}(\mathbf{x}, \boldsymbol{\epsilon})}{\partial \mathbf{x}}\right|_{\bar{\mathbf{x}}} \qquad \left.\begin{array}{l} \hat{\mathbf{H}}_1 = \left.\frac{\partial \hat{\mathbf{h}}_1(\hat{\mathbf{x}}_1)}{\partial \hat{\mathbf{x}}_1}\right|_{\bar{\mathbf{x}}} \\ \hat{\mathbf{H}}_2 = \left.\frac{\partial \hat{\mathbf{h}}_2(\hat{\mathbf{x}}_2)}{\partial \hat{\mathbf{x}}_2}\right|_{\bar{\mathbf{x}}} \\ \vdots \\ \hat{\mathbf{H}}_j = \left.\frac{\partial \hat{\mathbf{h}}_j(\hat{\mathbf{x}}_j)}{\partial \hat{\mathbf{x}}_j}\right|_{\bar{\mathbf{x}}} \end{array}\right\} \hat{\mathbf{H}} = \left.\frac{\partial \hat{\mathbf{h}}(\hat{\mathbf{x}})}{\partial \hat{\mathbf{x}}}\right|_{\bar{\mathbf{x}}} \tag{37}$$

such that $\mathbf{H_x}$ and $\hat{\mathbf{H}}$ can be expressed in terms of the individual vehicle measurement partials and noise being processed.

$$\mathbf{H_x} = \begin{bmatrix} \mathbf{H}_1 \\ \mathbf{H}_2 \\ \vdots \\ \mathbf{H}_j \end{bmatrix} \quad \hat{\mathbf{H}} = \begin{bmatrix} \hat{\mathbf{H}}_1 & \mathbf{0} & ... & \mathbf{0} \\ \mathbf{0} & \hat{\mathbf{H}}_2 & ... & \mathbf{0} \\ \vdots & \vdots & \ddots & \vdots \\ \mathbf{0} & \mathbf{0} & ... & \hat{\mathbf{H}}_j \end{bmatrix} \quad \mathbf{R} = \begin{bmatrix} \mathbf{R}_1 & \mathbf{0} & ... & \mathbf{0} \\ \mathbf{0} & \mathbf{R}_2 & ... & \mathbf{0} \\ \vdots & \vdots & \ddots & \vdots \\ \mathbf{0} & \mathbf{0} & ... & \mathbf{R}_j \end{bmatrix} \quad \hat{\mathbf{R}} = \begin{bmatrix} \hat{\mathbf{R}}_1 & \mathbf{0} & ... & \mathbf{0} \\ \mathbf{0} & \hat{\mathbf{R}}_2 & ... & \mathbf{0} \\ \vdots & \vdots & \ddots & \vdots \\ \mathbf{0} & \mathbf{0} & ... & \hat{\mathbf{R}}_j \end{bmatrix}$$

Combining expressions in Eqn 36 the augmented state update $\delta\mathbf{X}^+ = [\delta\mathbf{x}^+; \delta\hat{\mathbf{x}}^+]$ equation

$$\delta\mathbf{X}^+ = \mathbf{H}\delta\mathbf{X}^- + \mathbf{K}\boldsymbol{\epsilon} \tag{38}$$

where

$$\mathbf{H} = \begin{bmatrix} \mathbf{I} & \mathbf{0} \\ \hat{\mathbf{K}}\mathbf{H}_x & \mathbf{I} - \hat{\mathbf{K}}\hat{\mathbf{H}} \end{bmatrix} \qquad \mathbf{K} = \begin{bmatrix} \mathbf{0} \\ \hat{\mathbf{K}} \end{bmatrix}$$

such that the augmented state covariance matrix update $\mathbf{C}^+$ and the onboard state covariance matrix update $\hat{\mathbf{P}}^+$ become

$$\mathbf{C}^+ = \mathbf{H}\mathbf{C}^-\mathbf{H}^T + \mathbf{K}\mathbf{R}\mathbf{K}^T \tag{39}$$

$$\hat{\mathbf{P}}^+ = \left[\mathbf{I} - \hat{\mathbf{K}}\hat{\mathbf{H}}\right]\hat{\mathbf{P}}^-\left[\mathbf{I} - \hat{\mathbf{K}}\hat{\mathbf{H}}\right]^T + \hat{\mathbf{K}}\hat{\mathbf{R}}\hat{\mathbf{K}}^T \tag{40}$$

Correction Instantaneous translational maneuvers can be implemented in a linear covariance analysis by using a thruster model or using an accelerometer to estimate the burn imparted. For small velocity changes, the thruster model serves as a practical option. For larger burns, which in practice take more than several seconds to execute, incorporating the accelerometers into the filter is a more common approach. This section contains the mathematical formulation to capture the impacts of performing these impulsive maneuvers and *correcting* the augmented state and onboard navigation state covariance matrices. For simplicity, the thruster model is used to derive the *correction* equations. For cases when accelerometers are used in the loop to detect when to terminate the burn, see the following reference [12].

Impulsive translational burns directly affect the velocity states of the maneuvering vehicle, and they influence both the navigation and true dispersions, along with the onboard navigation error. The vehicle's inertial velocity is instantly *corrected* or changed based on the vehicle's true and navigation state prior to the burn $\mathbf{x}^{-c}$ and $\hat{\mathbf{x}}^{-c}$, the predicted velocity change $\Delta\hat{\mathbf{v}}$, and the actual imparted delta-v, $\Delta\mathbf{v}$. Let $\mathbf{N}_{\Delta v}$ be a $(n \times 3)$ matrix with zeros everywhere except for a (3×3) identity matrix corresponding to the inertial velocity states and allow $\hat{\mathbf{N}}_{\Delta v} = \hat{\mathbf{N}}_x\mathbf{N}_{\Delta v}$. The translational burn corrects the environment and navigation states as follows,

$$\left.\begin{array}{l} \mathbf{x}_1^{+c} = \mathbf{x}_1^{-c} + \mathbf{N}_{\Delta v}\Delta\mathbf{v}_1 \\ \mathbf{x}_2^{+c} = \mathbf{x}_2^{-c} + \mathbf{N}_{\Delta v}\Delta\mathbf{v}_2 \\ \vdots \\ \mathbf{x}_j^{+c} = \mathbf{x}_j^{-c} + \mathbf{N}_{\Delta v}\Delta\mathbf{v}_j \end{array}\right\} \mathbf{x}^{+c} = \mathbf{x}^{-c} + \mathbf{N}_{\Delta v}\Delta\mathbf{v} \qquad \left.\begin{array}{l} \hat{\mathbf{x}}_1^{+c} = \hat{\mathbf{x}}_1^{-c} + \hat{\mathbf{N}}_{\Delta v}\Delta\hat{\mathbf{v}}_1 \\ \hat{\mathbf{x}}_2^{+c} = \hat{\mathbf{x}}_2^{-c} + \hat{\mathbf{N}}_{\Delta v}\Delta\hat{\mathbf{v}}_2 \\ \vdots \\ \hat{\mathbf{x}}_j^{+c} = \hat{\mathbf{x}}_j^{-c} + \hat{\mathbf{N}}_{\Delta v}\Delta\hat{\mathbf{v}}_j \end{array}\right\} \hat{\mathbf{x}}^{+c} = \hat{\mathbf{x}}^{-c} + \hat{\mathbf{N}}_{\Delta v}\Delta\hat{\mathbf{v}} \tag{41}$$

The actual delta-v imparted on the vehicle in the inertial frame $\Delta\mathbf{v}$ due to an impulsive thrust is a function of the commanded delta-v in the inertial frame $\Delta\hat{\mathbf{v}}$, thruster noise $\boldsymbol{\eta}$, and the vehicle truth and navigation parameter states, $\mathbf{x}$ and $\hat{\mathbf{x}}$ respectively, to compensate for the vehicle's attitude errors, thruster bias, misalignment, and scale factor terms.

$$\left.\begin{array}{l} \Delta\mathbf{v}_1 = \mathbf{g}_1(\mathbf{x}, \hat{\mathbf{x}}_1, \Delta\hat{\mathbf{v}}_1, \boldsymbol{\eta}_1) \\ \Delta\mathbf{v}_2 = \mathbf{g}_2(\mathbf{x}, \hat{\mathbf{x}}_2, \Delta\hat{\mathbf{v}}_2, \boldsymbol{\eta}_2) \\ \vdots \\ \Delta\mathbf{v}_j = \mathbf{g}_j(\mathbf{x}, \hat{\mathbf{x}}_j, \Delta\hat{\mathbf{v}}_j, \boldsymbol{\eta}_j) \end{array}\right\} \Delta\mathbf{v} = \mathbf{g}(\mathbf{x}, \hat{\mathbf{x}}, \Delta\hat{\mathbf{v}}, \boldsymbol{\eta}) \qquad \left.\begin{array}{l} \Delta\hat{\mathbf{v}}_1 = \hat{\mathbf{g}}_1(\hat{\mathbf{x}}_1) \\ \Delta\hat{\mathbf{v}}_2 = \hat{\mathbf{g}}_2(\hat{\mathbf{x}}_2) \\ \vdots \\ \Delta\hat{\mathbf{v}}_j = \hat{\mathbf{g}}_j(\hat{\mathbf{x}}_j) \end{array}\right\} \Delta\hat{\mathbf{v}} = \hat{\mathbf{g}}(\hat{\mathbf{x}}) \tag{42}$$

The *correction* equations in Eqn 41 and Eqn 42 are linearized to produce the impulsive correction for both the true state dispersions $\delta\mathbf{x}^{+c}$, the navigation dispersions $\delta\hat{\mathbf{x}}^{+c}$, and the onboard navigation error $\delta\hat{\mathbf{e}}^{+c}$

$$\delta\mathbf{x}^{+c} = \left(\mathbf{I} + \mathbf{N}_{\Delta v}\mathbf{G}_x\right)\delta\mathbf{x}^{-c} + \mathbf{N}_{\Delta v}\left(\mathbf{G}_{\hat{x}} + \mathbf{G}_{\Delta\hat{v}}\hat{\mathbf{G}}_{\hat{x}}\right)\delta\hat{\mathbf{x}}^{-c} + \left(\mathbf{N}_{\Delta v}\mathbf{G}_\eta\right)\boldsymbol{\eta} \tag{43}$$

$$\delta\hat{\mathbf{x}}^{+c} = \left(\mathbf{I} + \hat{\mathbf{N}}_{\Delta v}\hat{\mathbf{G}}_{\hat{x}}\right)\delta\hat{\mathbf{x}}^{-c} \qquad \delta\hat{\mathbf{e}}^{+} = \left(\mathbf{I} + \hat{\mathbf{N}}_{\Delta v}\hat{\mathbf{G}}_{\hat{x}}\right)\delta\hat{\mathbf{e}}^{-c} - \left(\hat{\mathbf{N}}_{\Delta v}\hat{\mathbf{G}}_{\eta}\right)\hat{\boldsymbol{\eta}} \tag{44}$$

where $\hat{\mathbf{G}}_{\hat{x}}$ is the partial of the onboard targeting algorithm with respect to the navigation state.

$$\left.\begin{array}{l} \mathbf{G}_1 = \left.\frac{\partial \mathbf{g}_1(\mathbf{x},\hat{\mathbf{x}}_1,\Delta\hat{\mathbf{v}}_1,\boldsymbol{\eta}_1)}{\partial \mathbf{x}}\right|_{\bar{\mathbf{x}}} \\ \mathbf{G}_2 = \left.\frac{\partial \mathbf{g}_2(\mathbf{x},\hat{\mathbf{x}}_2,\Delta\hat{\mathbf{v}}_2,\boldsymbol{\eta}_2)}{\partial \mathbf{x}}\right|_{\bar{\mathbf{x}}} \\ \vdots \\ \mathbf{G}_j = \left.\frac{\partial \mathbf{g}_j(\mathbf{x},\hat{\mathbf{x}}_j,\Delta\hat{\mathbf{v}}_j,\boldsymbol{\eta}_j)}{\partial \mathbf{x}}\right|_{\bar{\mathbf{x}}} \end{array}\right\} \mathbf{G}_x = \left.\frac{\partial \mathbf{g}(\mathbf{x},\hat{\mathbf{x}},\Delta\hat{\mathbf{v}},\boldsymbol{\eta})}{\partial \mathbf{x}}\right|_{\bar{\mathbf{x}}} \qquad \left.\begin{array}{l} \hat{\mathbf{G}}_1 = \left.\frac{\partial \hat{\mathbf{g}}_1(\hat{\mathbf{x}}_1)}{\partial \hat{\mathbf{x}}_1}\right|_{\bar{\mathbf{x}}} \\ \hat{\mathbf{G}}_2 = \left.\frac{\partial \hat{\mathbf{g}}_2(\hat{\mathbf{x}}_2)}{\partial \hat{\mathbf{x}}_2}\right|_{\bar{\mathbf{x}}} \\ \vdots \\ \hat{\mathbf{G}}_j = \left.\frac{\partial \hat{\mathbf{g}}_j(\hat{\mathbf{x}}_j)}{\partial \hat{\mathbf{x}}_j}\right|_{\bar{\mathbf{x}}} \end{array}\right\} \hat{\mathbf{G}}_{\hat{x}} = \left.\frac{\partial \hat{\mathbf{g}}(\hat{\mathbf{x}}^{-c})}{\partial \hat{\mathbf{x}}}\right|_{\bar{\mathbf{x}}}$$

$$\left.\begin{array}{l} \mathbf{G}_{\hat{x}_1} = \left.\frac{\partial \mathbf{g}_1(\mathbf{x},\hat{\mathbf{x}}_1,\Delta\hat{\mathbf{v}}_1,\boldsymbol{\eta}_1)}{\partial \hat{\mathbf{x}}_1}\right|_{\bar{\mathbf{x}}} \\ \mathbf{G}_{\hat{x}_2} = \left.\frac{\partial \mathbf{g}_2(\mathbf{x},\hat{\mathbf{x}}_2,\Delta\hat{\mathbf{v}}_2,\boldsymbol{\eta}_2)}{\partial \hat{\mathbf{x}}_2}\right|_{\bar{\mathbf{x}}} \\ \vdots \\ \mathbf{G}_{\hat{x}_j} = \left.\frac{\partial \mathbf{g}_j(\mathbf{x},\hat{\mathbf{x}}_j,\Delta\hat{\mathbf{v}}_j,\boldsymbol{\eta}_j)}{\partial \hat{\mathbf{x}}_j}\right|_{\bar{\mathbf{x}}} \end{array}\right\} \mathbf{G}_{\hat{x}} = \left.\frac{\partial \mathbf{g}(\mathbf{x},\hat{\mathbf{x}},\Delta\hat{\mathbf{v}},\boldsymbol{\eta})}{\partial \hat{\mathbf{x}}}\right|_{\bar{\mathbf{x}}} \qquad \left.\begin{array}{l} \mathbf{G}_{\Delta\hat{v}_1} = \left.\frac{\partial \mathbf{g}_1(\mathbf{x},\hat{\mathbf{x}}_1,\Delta\hat{\mathbf{v}}_1,\boldsymbol{\eta}_1)}{\partial \Delta\hat{\mathbf{v}}_1}\right|_{\bar{\mathbf{x}}} \\ \mathbf{G}_{\Delta\hat{v}_2} = \left.\frac{\partial \mathbf{g}_2(\mathbf{x},\hat{\mathbf{x}}_2,\Delta\hat{\mathbf{v}}_2,\boldsymbol{\eta}_2)}{\partial \Delta\hat{\mathbf{v}}_2}\right|_{\bar{\mathbf{x}}} \\ \vdots \\ \mathbf{G}_{\Delta\hat{v}_j} = \left.\frac{\partial \mathbf{g}_j(\mathbf{x},\hat{\mathbf{x}}_j,\Delta\hat{\mathbf{v}}_j,\boldsymbol{\eta}_j)}{\partial \Delta\hat{\mathbf{v}}_j}\right|_{\bar{\mathbf{x}}} \end{array}\right\} \mathbf{G}_{\Delta\hat{v}} = \left.\frac{\partial \mathbf{g}(\mathbf{x},\hat{\mathbf{x}},\Delta\hat{\mathbf{v}},\boldsymbol{\eta})}{\partial \Delta\hat{\mathbf{v}}}\right|_{\bar{\mathbf{x}}}$$

Such that

$$\mathbf{G}_{\mathbf{x}} = \begin{bmatrix} \mathbf{G}_1 \\ \mathbf{G}_2 \\ \vdots \\ \mathbf{G}_j \end{bmatrix} \quad \mathbf{G}_{\hat{x}} = \begin{bmatrix} \mathbf{G}_{\hat{x}_1} & \mathbf{0} & \dots & \mathbf{0} \\ \mathbf{0} & \mathbf{G}_{\hat{x}_2} & \dots & \mathbf{0} \\ \vdots & \vdots & \ddots & \vdots \\ \mathbf{0} & \mathbf{0} & \dots & \mathbf{G}_{\hat{x}_j} \end{bmatrix} \quad \mathbf{G}_{\Delta\hat{v}} = \begin{bmatrix} \mathbf{G}_{\Delta\hat{v}_1} & \mathbf{0} & \dots & \mathbf{0} \\ \mathbf{0} & \mathbf{G}_{\Delta\hat{v}_2} & \dots & \mathbf{0} \\ \vdots & \vdots & \ddots & \vdots \\ \mathbf{0} & \mathbf{0} & \dots & \mathbf{G}_{\Delta\hat{v}_j} \end{bmatrix} \quad \hat{\mathbf{G}}_{\hat{x}} = \begin{bmatrix} \hat{\mathbf{G}}_1 & \mathbf{0} & \dots & \mathbf{0} \\ \mathbf{0} & \hat{\mathbf{G}}_2 & \dots & \mathbf{0} \\ \vdots & \vdots & \ddots & \vdots \\ \mathbf{0} & \mathbf{0} & \dots & \hat{\mathbf{G}}_j \end{bmatrix}$$

Combining expressions in Eqn 43, the augmented state correction $\delta\mathbf{X}^{+c} = [\delta\mathbf{x}^{+c}; \delta\hat{\mathbf{x}}^{+c}]$ equation is

$$\delta\mathbf{X}^{+c} = \mathbf{G}\delta\mathbf{X}^{-c} + \mathbf{N}\boldsymbol{\eta} \tag{45}$$

where

$$\mathbf{G} = \begin{bmatrix} \left(\mathbf{I} + \mathbf{N}_{\Delta v}\mathbf{G}_x\right) & \mathbf{N}_{\Delta v}\left(\mathbf{G}_{\hat{x}} + \mathbf{G}_{\Delta\hat{v}}\hat{\mathbf{G}}_{\hat{x}}\right) \\ \hat{\mathbf{N}}_x\mathbf{0}_x & \left(\mathbf{I} + \hat{\mathbf{N}}_{\Delta v}\hat{\mathbf{G}}_{\hat{x}}\right) \end{bmatrix} \qquad \mathbf{N} = \begin{bmatrix} \left(\mathbf{N}_{\Delta v}\mathbf{G}_\eta\right) \\ \mathbf{0}_{\hat{x}}\hat{\mathbf{N}}_{\Delta v} \end{bmatrix}$$

such that the augmented state covariance matrix update $\mathbf{C}^+$ is

$$\mathbf{C}^{+c} = \mathbf{G}\mathbf{C}^{-c}\mathbf{G}^T + \mathbf{N}\mathbf{S}_\eta\mathbf{N}^T \tag{46}$$

$$\hat{\mathbf{P}}^{+c} = \left(\mathbf{I} + \hat{\mathbf{N}}_{\Delta v}\hat{\mathbf{G}}_{\hat{x}}\right)\hat{\mathbf{P}}^{-c}\left(\mathbf{I} + \hat{\mathbf{N}}_{\Delta v}\hat{\mathbf{G}}_{\hat{x}}\right)^T + \left(\hat{\mathbf{N}}_{\Delta v}\hat{\mathbf{G}}_\eta\right)\hat{\mathbf{S}}_\eta\left(\hat{\mathbf{N}}_{\Delta v}\hat{\mathbf{G}}_\eta\right)^T \tag{47}$$

LOW LUNAR ORBIT TO NRHO RENDEZVOUS CONCEPT OF OPERATIONS

To highlight upcoming situations where multiple vehicles with a variety of simultaneously operating GN&C systems are required for baseline mission operations, this section provides details of a notional concept of operations for a phase of the NASA's Artemis III mission where a rendezvous scenario is initiated in low lunar orbit and terminates in a Near Rectilinear Halo Orbit. Following the successful lunar descent and

landing of a crewed HLS vehicle and completion of the lunar surface operations, HLS will ascend off the lunar surface to eventually re-rendezvous with the Orion spacecraft which has remained in the NRHO for the previous 7 days from the time HLS originally separated from Orion to depart from the NRHO towards the lunar surface.

Figure 5 illustrates an example of this re-rendezvous trajectory profile in the Earth-Moon Rotating (EMR) frame following the ascent of HLS from the lunar surface to a 15x100 km lunar orbit insertion through the initiation of re-rendezvous with Orion in the NRHO. The blue line highlights the HLS trajectory in low lunar orbit and the 12-hour transfer following the low lunar orbit departure (LLOD) burn to the designated NRHO re-rendezvous (NRR) location. The major translational burns, along with a variety of potential trajectory correction burns or NRHO acquisition (NRA) burns, are indicated with the solid red circles. The timing of when HLS performs each of these burns is also captured on the Orion profile (red line) with the solid gray dots. For this scenario, Orion is initially acting in the role of the passive target vehicle. The relative motion of the HLS lander with respect to the Orion spacecraft is also provided in Figure 6 where the relative trajectory is shown in the Sun-referenced local-vertical local-horizontal (S-LVLH) frame. The large dashed blue circle represents the range when the relative S-band measurements are acquired. The yellow star represents the direction to the sun, which by definition is always in the z-axis of the S-LVLH frame.

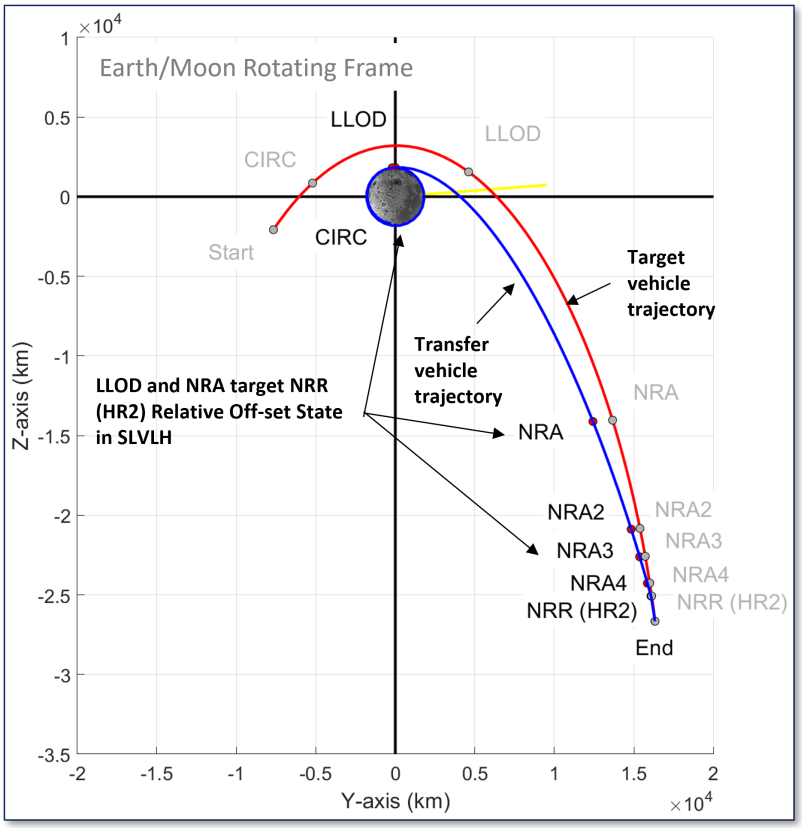

Figure 5. Simulated Rendezvous Trajectory Profile from Low Lunar Orbit to the NRHO in the Earth-Moon Rotating Frame.

The remainder of this section will outline the major concept of operations in terms of events, scheduling, guidance and targeting strategies, and sensor utilization for the NRHO rendezvous scenario.

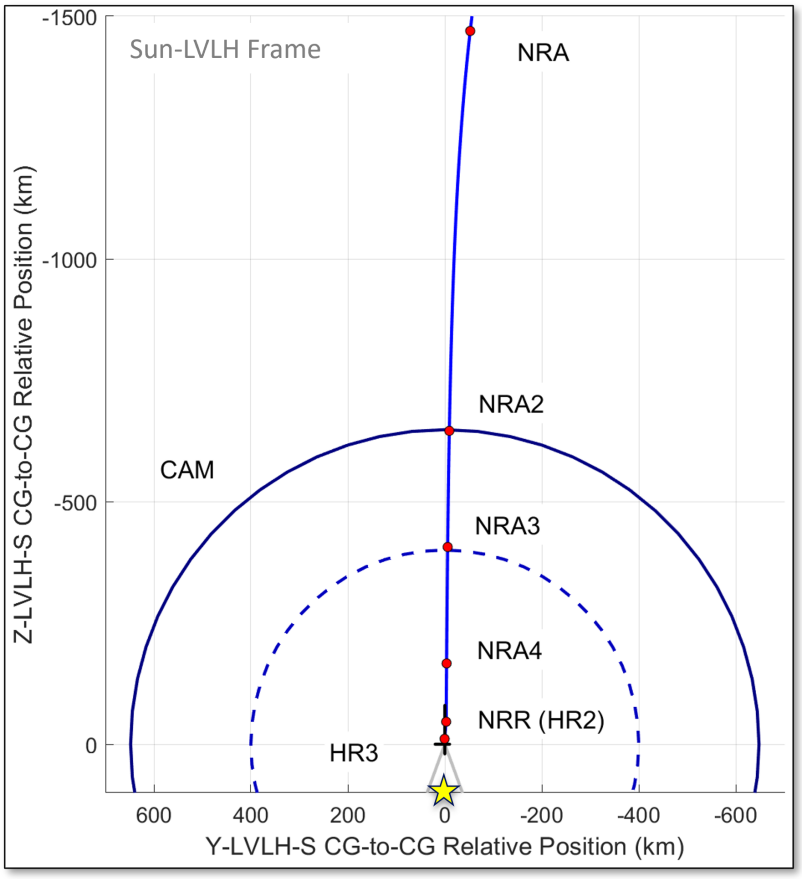

Figure 6. Simulated Rendezvous Trajectory Profile from Low Lunar Orbit to the NRHO in the Sun-referenced LVLH Frame.

Concept of Operations

A summary of the timeline and concept of operations for this analysis is outlined in Table 1. Once Orion reaches the proper phase in the NRHO, the HLS lunar lander will ascend off the lunar surface in preparation for an eventual docking with Orion. This baseline assumption that both vehicles are able to communicate with the ground and replan events to accommodate any potential deviations of Orion while remaining in the NRHO is reflected in the current analysis. It implies Orion does not need to perform significant orbit maintenance burns in the NRHO and can largely adopt the role of a passive target vehicle. For contingency cases where there is a permanent communication loss with the ground, Orion will likely need to actively perform burns to remain close to the predesignated reference NRHO trajectory and transition location.

Following ascent, HLS inserts into an initial 15x100 km lunar orbit. Approximately 55 minutes later, HLS executes a circularization burn that places the vehicle in a 100x100 km orbit. Although there are inevitable trades as to whether HLS does a single revolution in low lunar orbit, performs multiple orbits, or none at all; the results shown in this paper reflect a single revolution. Consequently, almost three hours after ascent, HLS performs the low lunar orbit departure (LLOD) burn and is placed on a transfer trajectory to insert into the NRHO about 12-hours later. The LLOD burn is performed using a two-level targeting algorithm that aims to hit a relative offset point to Orion in the NRHO.

During this transit, several trajectory correction burns can be performed to support transition requirements for subsequent rendezvous and close proximity operations. The initial NRHO acquisition (NRA) or trajectory correction burn is performed 6 hours after LLOD. It uses the absolute state data uplinked from the ground

Table 1. Concept of Operations for Orion-HLS Re-Rendezvous

Event	Description	MET	Targeting	Sensors
LOI	15x100 km Lunar Orbit Insertion	00:00:00	TLT (LLOD Inrt Pos)	IMU, Startracker, DSN
CIRC	100x100 km Circularization Burn	00:54:07	TLT (LLOD Inrt Pos)	IMU, Startracker, DSN
LLOD	Low Lunar Orbit Departure Burn	02:49:48	TLT (NRR Rel Pos)	IMU, Startracker, DSN
NRA	NRHO Acquisition (Correction) #1	08:47:42	NRT (NRR Rel Pos)	IMU, Startracker, DSN
NRA2	NRHO Acquisition (Correction) #2	12:17:42	NRT (NRR Rel Pos)	IMU, Startracker, DSN, S-band
NRA3	NRHO Acquisition (Correction) #3	13:17:42	NRT (NRR Rel Pos)	IMU, Startracker, DSN, S-band
NRA4	NRHO Acquisition (Correction) #4	14:17:42	NRT (NRR Rel Pos)	IMU, Startracker, DSN, S-band
NRR	NRHO Re-Rendezvous Burn	14:47:42	NRT (NRR Rel Vel)	IMU, Startracker, DSN, S-band
TRANS	Transition Point	15:47:42	—-	IMU, Startracker, DSN, S-band

for both vehicles to target the designated relative offset for the NRHO re-rendezvous point (NRR). To take advantage of relative S-band range and range-rate measurements between both vehicles, NRA2-NRA4 are strategically located within the S-band range to allow targeted burns to take advantage of this additional relative information. Each of these correction burns are spaced out by one hour increments. The final NRHO re-rendezvous burn, NRR, nulls the relative velocity between the two vehicles such that an hour later, a formal transition occurs where Orion becomes the active chaser vehicle and HLS becomes a passive target vehicle.

Targeting Algorithms

To support rendezvous and docking requirements, the relative trajectory dispersions must be constrained to a specific tolerance, whereas, the inertial dispersions may be noticeably larger. Not only do the inertial and relative navigation errors impact performance, but the selection of utilizing inertial or relative targeting can also significantly impact performance results. The inertial and relative targeting algorithms used to support rendezvous from low lunar orbit to NRHO insertion for re-rendezvous activities include a two-level targeter (TLT) and an NRHO relative targeting (NRT) algorithm.

Two-Level Targeter (TLT) The departure burn from the NRHO to low-lunar orbit (LLO) along with the low-lunar orbit maintenance burns are executed with an impulsive constrained two-level targeter that uses a two-level corrections process to target the desired lunar orbit insertion (LOI) state and the de-orbit insertion (DOI) state [13–17]. The algorithm works by dividing the trajectory into segments, or a series of intermediate targets known as patch states. The first stage, or the level-I process, introduces impulsive maneuvers at the interior patch states until position continuity across all segments is achieved. The second stage, or the level-II process, adjusts the shape of the trajectory by spatially and temporally relocating the patch states to drive the velocity discontinuities to zero.

NRHO Relative Targeting (NRT) The NRHO relative targeting (NRT) algorithm used for this study is an iterative method that accounts for the inertial propagation of both the chaser and target vehicle in a multi-body gravitational field. The algorithm ultimately targets a specific relative position offset to the target vehicle at the final transfer time.

Inertial and Relative Sensor Models

Typically a vehicle incorporates both primary and backup navigation systems designated to support baseline operations, but also to account for any potential contingencies. This study only focuses on the primary navigation system, which consists of DSN ground updates for both HLS and Orion, accelerometers, gyros, star trackers, and S-band relative range and range-rate measurements. The mathematical models used for the different measurement types are provided below.

DSN Ground Update The Deep Space Network (DSN) ground update provides a position and velocity state estimate and covariance to both the HLS lander and Orion spacecraft at designated epochs based on range $\tilde{\rho}$ and doppler measurements $\tilde{\dot{\rho}}$ between the ground tracking station and the respective spacecraft [18], which are functions of the vehicle's inertial position $\mathbf{r}_l^i$, the vehicle's mounted antenna location $\mathbf{r}_a^b$, vehicle's inertial-to-body transformation matrix $\mathbf{T}_b^i$, the vehicle's angular rate $\boldsymbol{\omega}_l^b$, the inertial-to-planet transformation $\mathbf{T}_p^i$, the Earth's angular rate $\boldsymbol{\omega}_e^p$, the ground station location $\mathbf{r}_{gs}^p$ in the planet-fixed frame, the range bias $\boldsymbol{b}_\rho$, doppler bias $\boldsymbol{b}_{\dot{\rho}}$, range noise $\boldsymbol{\upsilon}_\rho$, and doppler noise $\boldsymbol{\upsilon}_{\dot{\rho}}$.

$$\tilde{\rho} = \left|\mathbf{r}_l^i + \mathbf{T}_b^i \mathbf{r}_a^b - \mathbf{T}_p^i \mathbf{r}_{gs}^p\right| + \boldsymbol{b}_\rho + \boldsymbol{\upsilon}_\rho \tag{48}$$

$$\tilde{\dot{\rho}} = \frac{\left[\mathbf{v}_l^i + \mathbf{T}_b^i\left(\boldsymbol{\omega}_l^b \times \mathbf{r}_a^b\right) - \mathbf{T}_p^i\left(\boldsymbol{\omega}_e^p \times \mathbf{r}_{gs}^p\right)\right]^{\mathrm{T}}\left[\mathbf{r}_l^i + \mathbf{T}_b^i \mathbf{r}_a^b - \mathbf{T}_p^i \mathbf{r}_{gs}^p\right]}{\left[\mathbf{r}^i + \mathbf{T}_b^i \mathbf{r}_a^b - \mathbf{T}_p^i \mathbf{r}_{gs}^p\right]} + \boldsymbol{b}_{\dot{\rho}} + \boldsymbol{\upsilon}_{\dot{\rho}} \tag{49}$$

The uncertainty parameters used for the DSN ground updates for both Orion and HLS spacecraft are given in Table 2 and Table 3, respectively.

Accelerometer The accelerometer measures the non-gravitational acceleration in the IMU case frame $\tilde{\mathbf{a}}^{imu}$, which is a function of the nominal inertial-to-body transformation matrix $\bar{\mathbf{T}}_i^b$, the nominal body-to-IMU transformation $\bar{\mathbf{T}}_b^{imu}$, the actual attitude dispersion $\boldsymbol{\theta}$, the misalignment $\boldsymbol{\mu}_a$, the constant scale factor $\mathbf{s}_a$, the Markov scale factor $\boldsymbol{\sigma}_a$, the constant bias $\mathbf{b}_a$, the Markov bias $\boldsymbol{\beta}_a$, the nonorthogonality factor $\boldsymbol{\gamma}_a$, and the velocity random walk (noise) $\boldsymbol{\upsilon}_a$.

$$\tilde{\mathbf{a}}^{imu} = \left(\mathbf{I} + [(\mathbf{s}_a + \boldsymbol{\sigma}_a)\diagdown]\right)\left[\left(\mathbf{I} + [\boldsymbol{\mu}_a\times]\right)\left(\mathbf{I} + [\boldsymbol{\gamma}_a *]\right)\bar{\mathbf{T}}_b^{imu}\left(\mathbf{I} + [\boldsymbol{\theta}\times]\right)\bar{\mathbf{T}}_i^b \mathbf{a}^i + \mathbf{b}_a + \boldsymbol{\beta}_a + \boldsymbol{\upsilon}_a\right] \tag{50}$$

The uncertainty parameters used for the accelerometer are listed in Table 5.

Gyro The gyros measure the vehicle's angular rates in the IMU case frame $\tilde{\boldsymbol{\omega}}^{imu}$ and is represented as a function of the nominal body-to-IMU transformation $\bar{\mathbf{T}}_b^{imu}$ where b indicates the vehicle body-fixed frame, the misalignment $\boldsymbol{\mu}_\omega$, the constant scale factor $\mathbf{s}_\omega$, the Markov scale factor $\boldsymbol{\sigma}_\omega$, the constant bias $\mathbf{b}_\omega$, the Markov bias $\boldsymbol{\beta}_\omega$, the nonorthogonality factor $\boldsymbol{\gamma}_\omega$, and the angular random walk (noise) $\boldsymbol{\upsilon}_\omega$.

$$\tilde{\boldsymbol{\omega}}^{imu} = \left(\mathbf{I} + [(\mathbf{s}_\omega + \boldsymbol{\sigma}_\omega)\diagdown]\right)\left[\left(\mathbf{I} + [\boldsymbol{\mu}_\omega\times]\right)\left(\mathbf{I} + [\boldsymbol{\gamma}_\omega *]\right)\bar{\mathbf{T}}_b^{imu}\boldsymbol{\omega}^b + \mathbf{b}_\omega + \boldsymbol{\beta}_\omega + \boldsymbol{\upsilon}_\omega\right] \tag{51}$$

The uncertainty parameters used for the gyroscope are listed in Table 6.

Star Tracker The star tracker provides an accurate measurement of the vehicle's orientation. The generated inertial-to-star tracker quaternion is a function of the body-to-star tracker mounting $\mathbf{q}_b^{st}$, the actual inertial-to-body quaternion $\mathbf{q}_i^b$, the sensor bias $\mathbf{b}_{st}$, noise $\boldsymbol{\eta}_{st}$, and misalignment $\boldsymbol{\mu}_{st}$

$$\tilde{\mathbf{q}}_{st}^i = \mathbf{q}(\boldsymbol{\eta}_{st}) \otimes \mathbf{q}(\mathbf{b}_{st}) \otimes \mathbf{q}(\boldsymbol{\eta}_{st}) \otimes \mathbf{q}_b^{st} \otimes \mathbf{q}_i^b \tag{52}$$

The star tracker parameters are summarized in Table 7.

S-band Relative Range and Range-Rate The relative range $\tilde{\rho}_{rel}$ and range-rate $\tilde{\dot{\rho}}_{rel}$ measured between the two rendezvousing vehicles' S-band systems is modeled as a function of the chaser vehicle's inertial position $\mathbf{r}_c^i$, the chaser vehicle's inertial velocity $\mathbf{v}_c^i$, the target vehicle's inertial position $\mathbf{r}_t^i$, the target vehicle's inertial velocity $\mathbf{v}_t^i$, the relative range bias $\boldsymbol{b}_{\rho_{rel}}$, the relative range-rate bias $\boldsymbol{b}_{\dot{\rho}_{rel}}$, the relative range noise $\boldsymbol{\upsilon}_{\rho_{rel}}$, and the relative range-rate noise $\boldsymbol{\upsilon}_{\dot{\rho}_{rel}}$.

$$\tilde{\rho}_{rel} = \left|\mathbf{r}_c^i - \mathbf{r}_t^i\right| + \boldsymbol{b}_{\rho_{rel}} + \boldsymbol{\upsilon}_{\rho_{rel}} \tag{53}$$

$$\tilde{\dot{\rho}}_{rel} = \left|\mathbf{v}_c^i - \mathbf{v}_t^i\right| + \boldsymbol{b}_{\dot{\rho}_{rel}} + \boldsymbol{\upsilon}_{\dot{\rho}_{rel}} \tag{54}$$

The relative range and range-rate parameters are summarized in Table 4.

Table 2. Orion DSN

Parameter	3σ
Range Noise, m	25
Range-rate Noise, cm/s	1.5
Range Bias, m	25
Range-rate Bias, cm/s	1.5
Elevation Mask, deg	10.0
Max Pass Duration, hr	2.0

Table 3. HLS DSN

Parameter	3σ
Range Noise, m	25
Range-rate Noise, cm/s	1.5
Range Bias, m	25
Range-rate Bias, cm/s	1.5
Elevation Mask, deg	10.0
Max Pass Duration, hr	2.0

Table 4. HLS Relative S-band

Parameter	3σ
Range Noise, m	25
Range-rate Noise, cm/s	1.5
Range Bias, m	25
Range-rate Bias, cm/s	1.5
Max Range, km	800
Meas Interval, sec	10.0

Table 5. HLS Accelerometer [19]

Parameter	3σ
VRW, mm/s/sqrt(s)	0.3
Bias, μg	84
Scale Factor, ppm	450
Nonorthogonal, arcsec	17
Markov Bias, μg	84
Markov SF, ppm	450

Table 6. HLS Gyros [19]

Parameter	3σ
ARW, deg/$\sqrt{hr}$	0.015
Bias, deg/hr	0.036
Scale Factor, ppm	27
Nonorthogonal, arcsec	19
Markov Bias, deg/hr	0.036
Markov SF, ppm	27

Table 7. HLS Startracker [19]

Parameter	3σ
Boresight Noise, arcsec	72
Crs-Boresight Bias, arcsec	24
Misalignment, deg	0.5

Table 8. Process Noise

Parameter	3σ
Orion Trans, m/s/$\sqrt{s}$	$0.42e^{-3}$
HLS Trans, m/s/$\sqrt{s}$	$0.42e^{-3}$
Orion Rot, rad/s/$\sqrt{s}$	$0.0e^{-6}$
HLS Rot, rad/s/$\sqrt{s}$	$0.0e^{-6}$

Table 9. Orion Initial Disp

Parameter	3σ
Position, km	2
Velocity, cm/s	20
Attitude, deg	0.5
Attitude-Rate, deg/s	0.01

Table 10. Orion Initial Nav

Parameter	3σ
Position, km	2
Velocity, cm/s	2
Attitude, deg	0.05
Attitude-Rate, deg/s	0.01

Table 11. HLS Initial Disp

Parameter	3σ
Position, km	2
Velocity, cm/s	20
Attitude, deg	0.5
Attitude-Rate, deg/s	0.01

Table 12. HLS Initial Nav

Parameter	3σ
Position, km	2
Velocity, cm/s	2
Attitude, deg	0.05
Attitude-Rate, deg/s	0.01

Table 13. HLS Thrusters

Parameter	3σ
Bias, cm/s	8
Noise, cm/s	8
Scale Factor, ppm	7000
Misalignment, deg	0.1

EVALUATION OF PERFORMANCE FROM LOW LUNAR ORBIT TO NRHO RENDEZVOUS

Given the capability to model multiple vehicles with multiple GN&C systems that are estimating the states of multiple vehicles, this section utilizes these tools to begin investigating the integrated performance of two rendezvousing vehicles in an NRHO. Although an assortment of contingencies and off-nominal scenarios could be evaluated, only the baseline configuration is considered to produce preliminary results to determine the anticipated performance for a notional Artemis III flight phase when an HLS lander ascends from the lunar surface to eventually rendezvous with the Orion spacecraft. Results are shown for ground tracking performance, relative trajectory dispersions, the relative position and velocity dispersions and navigation errors, and the total delta-v usage (nominal plus 3-sigma dispersions).

Ground Tracking Performance The DSN ground tracking performance for both Orion and HLS are provided in Figure 7 and Figure 8, respectively. There are essentially two separate and independent ground tracking filters that estimate the inertial position and velocity of each spacecraft and that are uplinked to support designated translational burns at key epochs.

The ground tracking coverage for Orion, Orion's visibility from each ground station, and the resulting ground navigation performance are provided in Figure 7(a), Figure 7(b), and Figure 7(c) respectively. For Orion, only 3 ground stations are utilized, so there are intervals where only one is visible. As a result, the uncertainty in Orion's inertial position and velocity estimate increases only to be reduced again when a second ground station comes within view. Ultimately, by NRR Orion's inertial position can be determined within 3-5 km.

The equivalent performance plots for the HLS vehicle ground tracking are provided in Figure 8(a), Figure 8(b), and Figure 8(c). In this instance, it is assumed that 9 ground stations are available to track the lunar lander. So although the translating HLS vehicle is more difficult to initially track than the quiescent Orion spacecraft, the additional ground stations allow HLS's inertial position to be determined within 1-2 km at NRR.

Relative Trajectory Dispersions One of the critical performance metrics for rendezvous and docking is how well both vehicles perform to ensure the relative trajectory dispersions adequately remain within specifications to support the crucial proximity operations. Figure 9 highlights the nominal relative trajectory profile of HLS to Orion in the Sun-referenced LVLH frame (blue line) along with the expected 3-sigma deviations from the nominal (maroon ellipses). The solid and dashed circles represent ranges of 400 km and 800 km, respectively, to indicate when the S-band relative range and range-rate measurements may be available. In addition, pivotal translational burns or epochs are indicated with a solid red dot and labeled so that intuition of when they occur with regards to the trajectory profile can be established.

Figure 9(a) provides the end-to-end relative motion plot from shortly after lunar ascent to the NRHO rendezvous transition point in the S-LVLH frame in the YZ-plane. Although the relative profile may not be intuitive initially, it can be compared to the plots in Figure 5 to gain more insight. For this particular launch epoch from the lunar surface, HLS approaches Orion following the first major trajectory correction burn (NRA) such that HLS comes from the negative z-direction. Since the S-LVLH z-axis is always directed towards the Sun, this implies HLS is visible to Orion for a significant portion of the lunar transfer phase prior to the HLS inserting into the NRHO and performing the NRR burn. This is not always the case and will vary with the selected launch epoch.

Figure 9(b) zooms in on the relative trajectory to capture the NRA burn through the NRR transition burn which essentially inserts HLS into the NRHO and initiates the transition of HLS being the active target vehicle to the passive chaser vehicle. Notice the relative trajectory dispersions funnel to the relative NRR point due to the relative targeting scheme employed and the accurate navigation provided from both the DSN tracking of both vehicles. The accurate ranging information available by S-band within 400-800 km also contributes to the performance. The notional placement of NRA2-NRA4 becomes more apparent in this context as these burns can utilize information extracted from the S-band system to support the relative targeting.

Relative Navigation Errors and Dispersions The time history and numerical details of both the relative trajectory dispersions and the relative navigation errors are given in Figure 10. Figure 10(a) focuses on the relative dispersions with the relative position, velocity, and attitude time history 3-sigma dispersions shown in the plots on the left and the specific numerical values at key epochs provided in tabulated form at the top right of the figure. Both the magnitude as well as components along the line-of-sight (LOS), out-of-plane normal (OOP), and in-plane normal (IPN) are provided. The relative trajectory profile and corresponding dispersions in the S-LVLH frame near the NRR burn is also included to give a geometrical context to the current rendezvous problem. One relevant observation is that when HLS inserts into the NRHO and for the subsequent hour, the relative 3-sigma position dispersions are less than 4.5 km with a relative velocity 3-sigma dispersion within 0.15 m/s.

The relative navigation errors are emphasized in Figure 10(b). The data is presented similarly to the trajectory dispersions where the relative position, velocity, and attitude time history navigation errors are

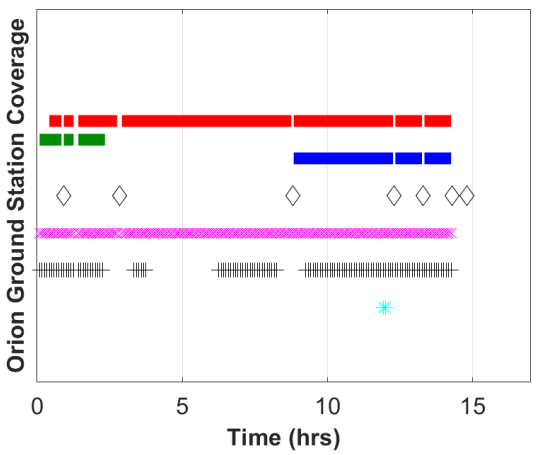

(a) Orion Coverage

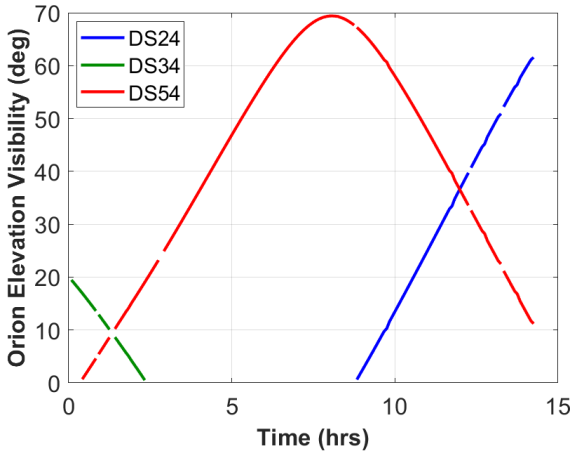

(b) Orion Visibility

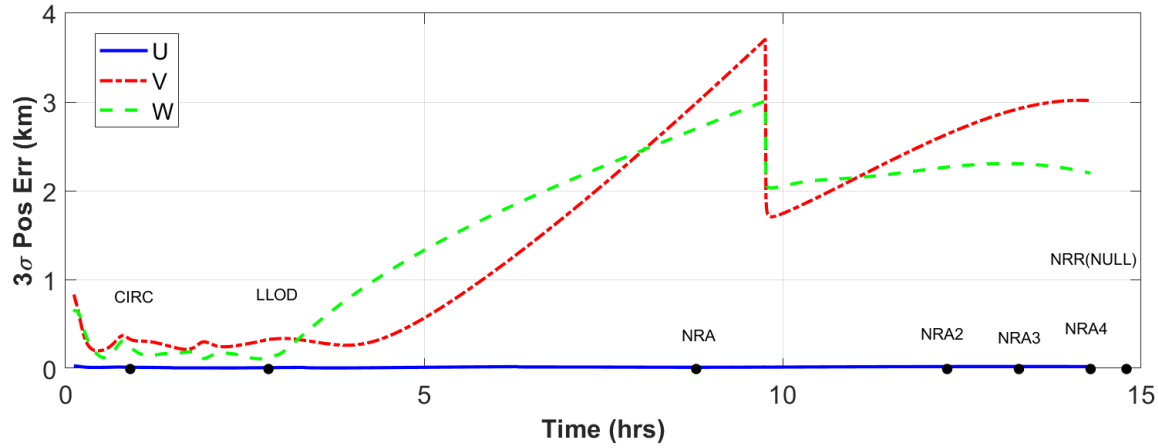

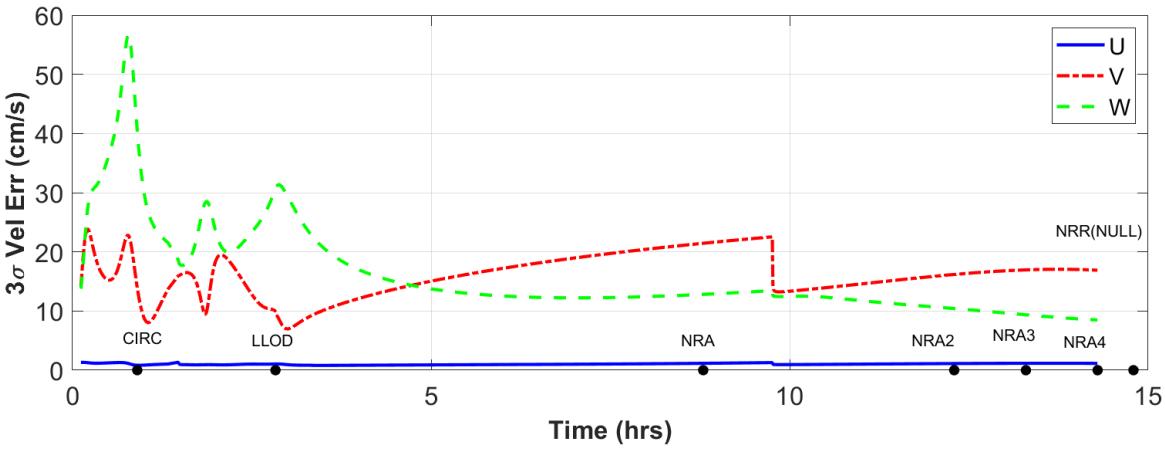

(c) Orion Performance

Figure 7. Orion Ground Tracking Performance

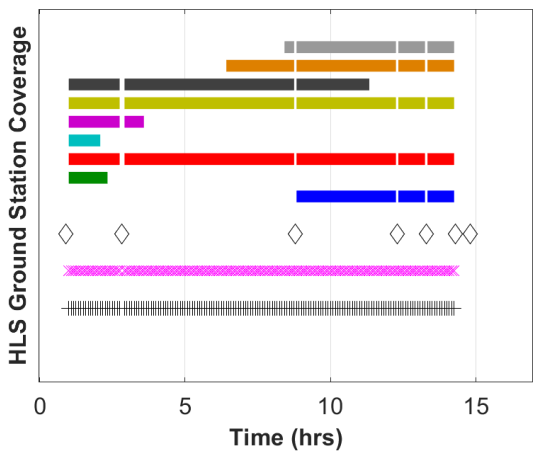

(a) HLS Coverage

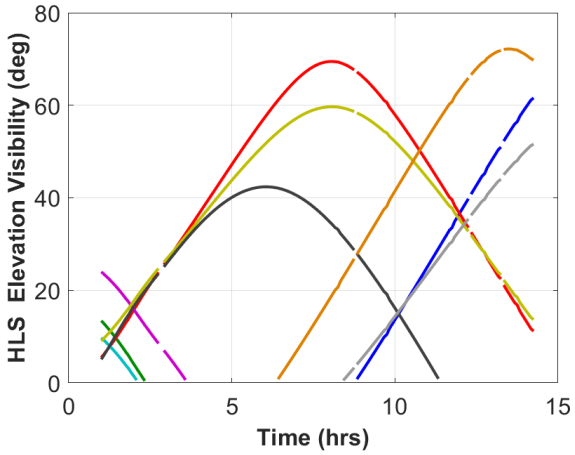

(b) HLS Visibility

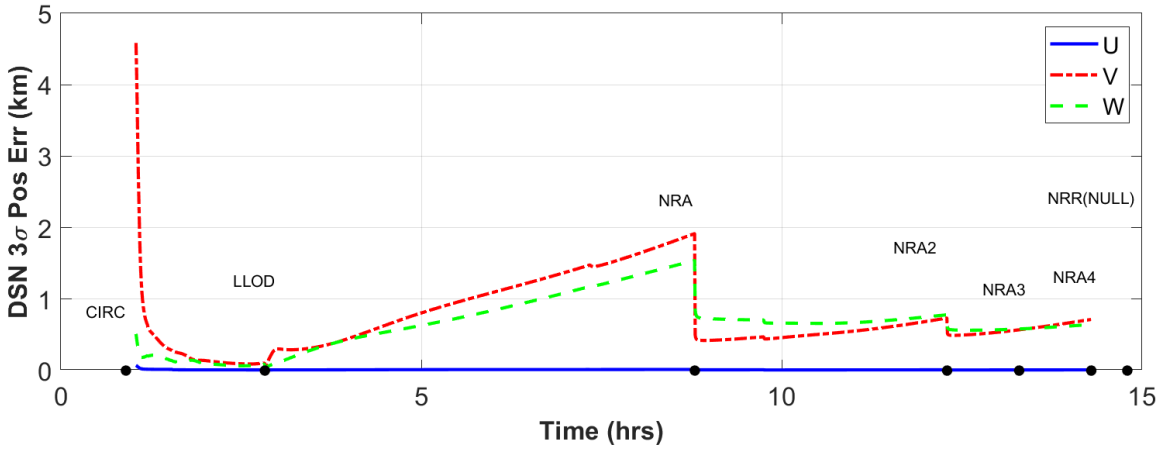

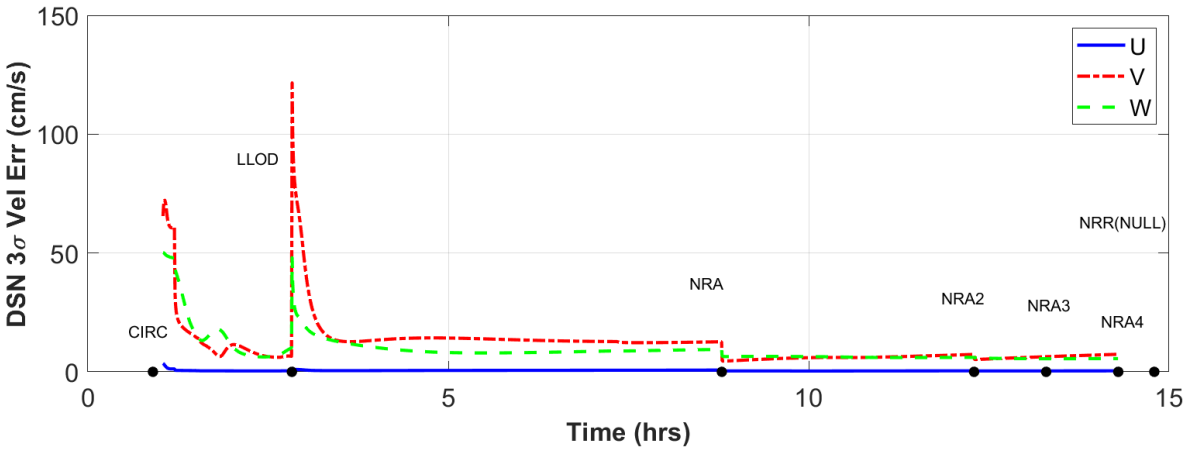

(c) HLS Performance

Figure 8. HLS Ground Tracking Performance

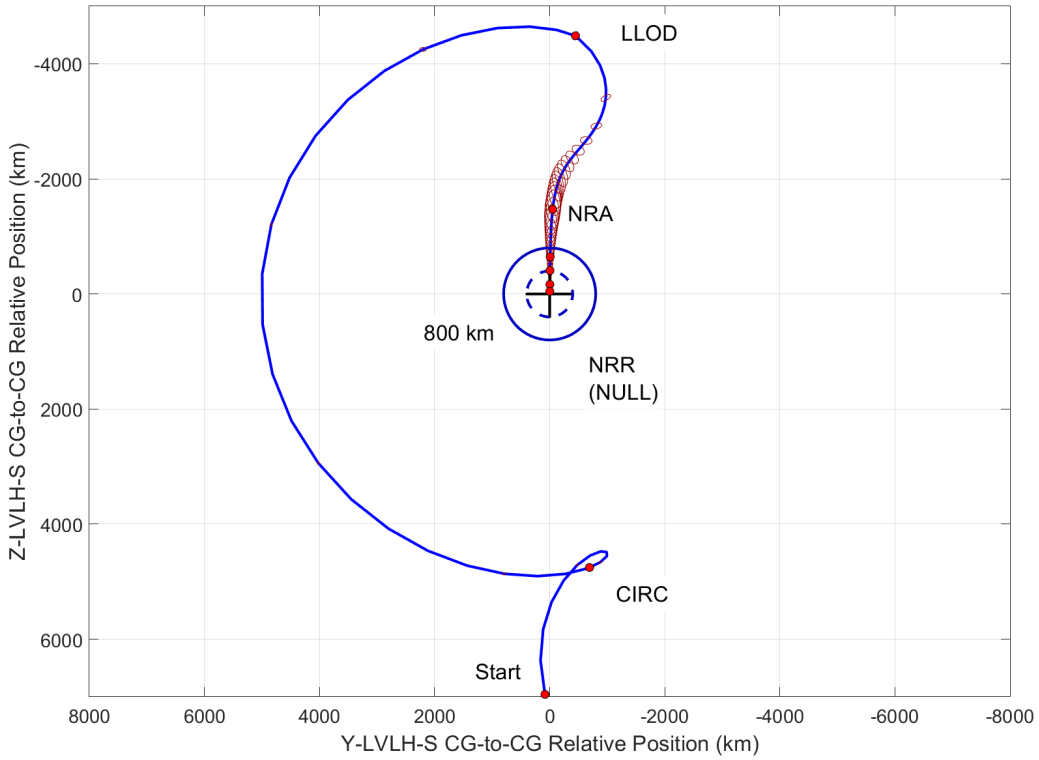

(a) Trajectory Dispersions from Lunar Ascent to Transition Point

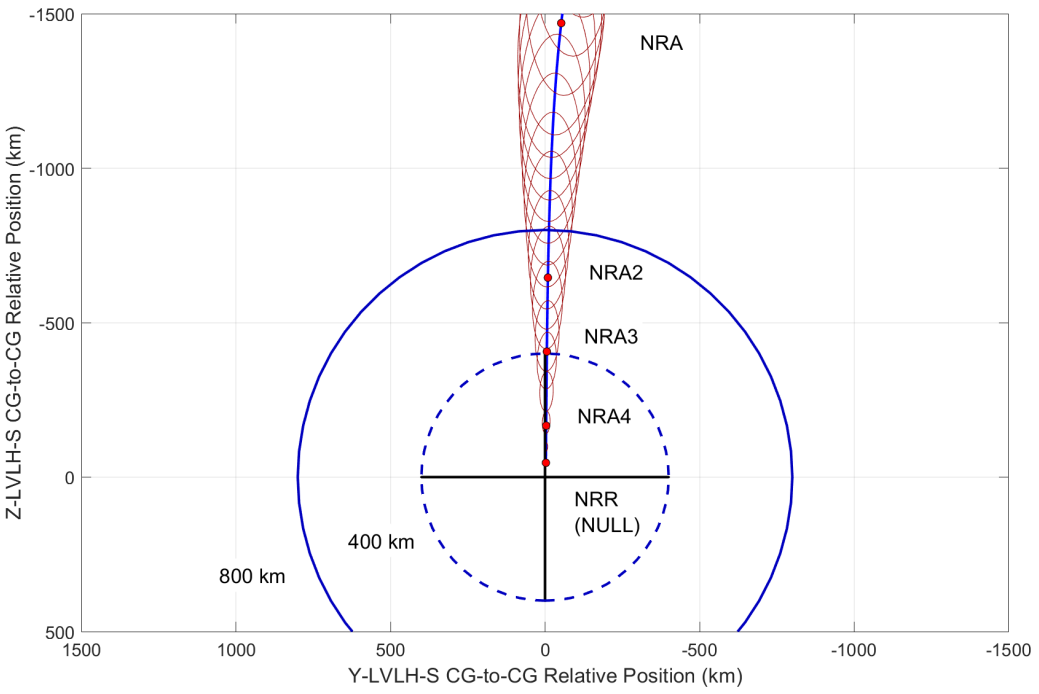

(b) Trajectory Dispersions from Initial Trajectory Correction Burn to Transition Point

Figure 9. Relative Trajectory Dispersions in Sun-Referenced LVLH Frame

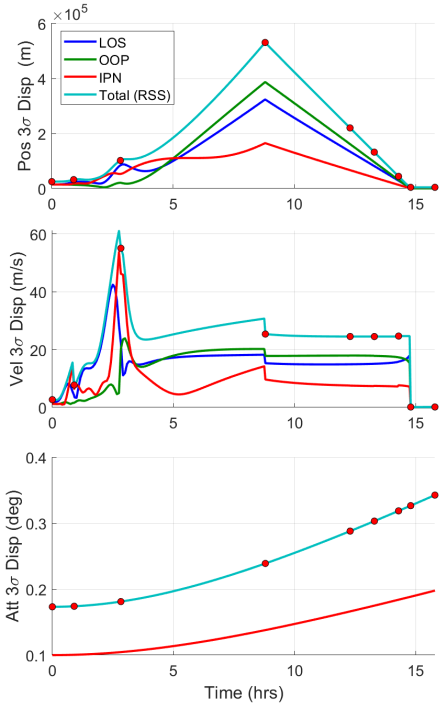

Event Name	Sim Elapsed Time (h:mm:ss)	3-sig LOS Pos Disp (m)	3-sig OOP Pos Disp (m)	3-sig IPN Pos Disp (m)	3-sig |Pos| Disp (m)	3-sig LOS Vel Disp (m/s)	3-sig OOP Vel Disp (m/s)	3-sig IPN Vel Disp (m/s)	3-sig |Vel| Disp (m/s)	3-sig X Att Disp (deg)	3-sig Y Att Disp (deg)	3-sig Z Att Disp (deg)	3-sig |Att| Disp (deg)
Start	0:00:00	14437.7	14434.7	14434.3	25003.1	2.057	1.205	1.224	2.680	0.100	0.100	0.100	0.173
CIRC	0:54:07	22907.9	13570.8	18055.5	32170.5	4.066	1.610	6.392	7.744	0.100	0.100	0.100	0.174
LLOD	2:49:48	84577.8	20964.7	52870.8	101922.8	22.086	20.283	46.123	55.013	0.105	0.105	0.105	0.181
NRA	8:47:42	323845.8	387196.3	165013.0	531061.5	15.271	17.787	9.633	25.345	0.138	0.138	0.138	0.239
NRA2	12:17:42	134214.1	161497.0	66670.8	220317.3	14.902	17.932	7.527	24.501	0.166	0.166	0.166	0.288
NRA3	13:17:42	81418.0	96177.6	39813.6	132152.0	15.074	17.804	7.438	24.485	0.175	0.175	0.175	0.303
NRA4	14:17:42	28414.7	31118.8	13280.6	44183.1	15.830	17.290	7.641	24.656	0.184	0.184	0.184	0.319
NRR	14:47:42	2392.8	358.5	3406.6	4178.4	0.029	0.046	0.109	0.122	0.188	0.188	0.188	0.326
End	15:47:42	2403.0	432.0	3497.2	4265.1	0.050	0.062	0.117	0.142	0.198	0.198	0.198	0.342

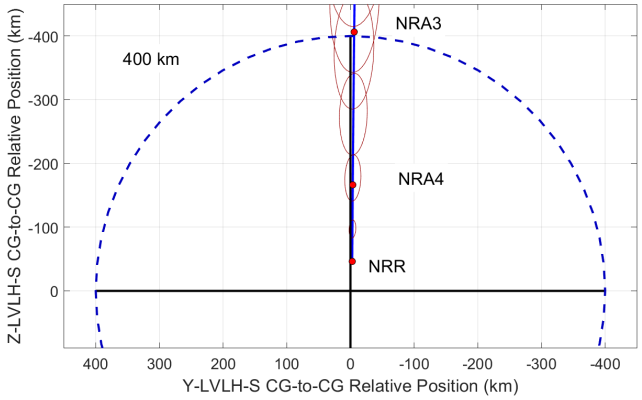

(a) Relative Trajectory Dispersions

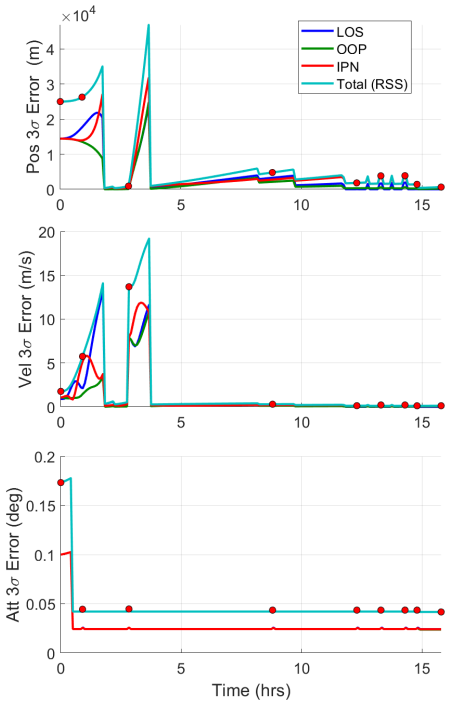

Event Name	Sim Elapsed Time (h:mm:ss)	3-sig LOS Pos Err (m)	3-sig OOP Pos Err (m)	3-sig IPN Pos Err (m)	3-sig |Pos| Err (m)	3-sig LOS Vel Err (m/s)	3-sig OOP Vel Err (m/s)	3-sig IPN Vel Err (m/s)	3-sig |Vel| Err (m/s)	3-sig X Att Err (deg)	3-sig Y Att Err (deg)	3-sig Z Att Err (deg)	3-sig |Att| Err (deg)
Start	0:00:00	14434.5	14434.5	14434.1	25001.1	0.898	1.070	1.068	1.759	0.100	0.100	0.100	0.173
CIRC	0:54:07	17659.9	13546.9	13949.8	26267.6	2.119	1.445	5.147	5.750	0.026	0.026	0.026	0.044
LLOD	2:49:48	735.5	93.0	522.2	906.8	7.909	7.895	7.907	13.690	0.026	0.026	0.026	0.045
NRA	8:47:42	3281.9	2125.1	2761.8	4786.9	0.202	0.118	0.183	0.297	0.025	0.025	0.025	0.044
NRA2	12:17:42	22.8	301.6	1804.5	1829.7	0.023	0.038	0.121	0.129	0.025	0.025	0.025	0.044
NRA3	13:17:42	1655.3	533.8	3424.8	3841.1	0.127	0.048	0.163	0.212	0.025	0.025	0.025	0.044
NRA4	14:17:42	1900.9	557.2	3340.8	3884.0	0.141	0.050	0.150	0.212	0.025	0.025	0.025	0.044
NRR(NULL)	14:47:42	37.0	209.9	1402.7	1418.9	0.029	0.046	0.109	0.122	0.025	0.025	0.025	0.044
End	15:47:42	18.0	220.6	594.6	634.5	0.001	0.061	0.108	0.124	0.024	0.024	0.024	0.042

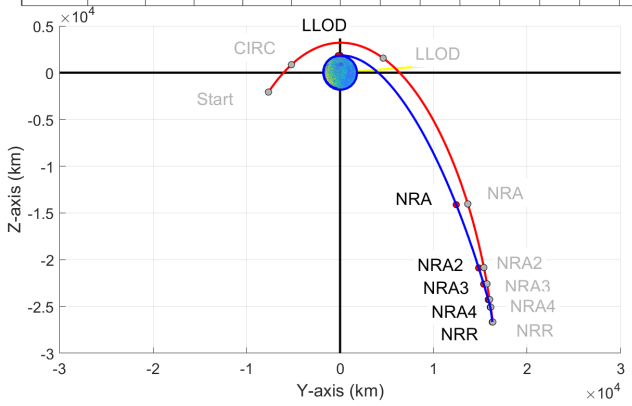

(b) Relative Navigation Errors

Figure 10. Relative Navigation Errors and Trajectory Dispersions

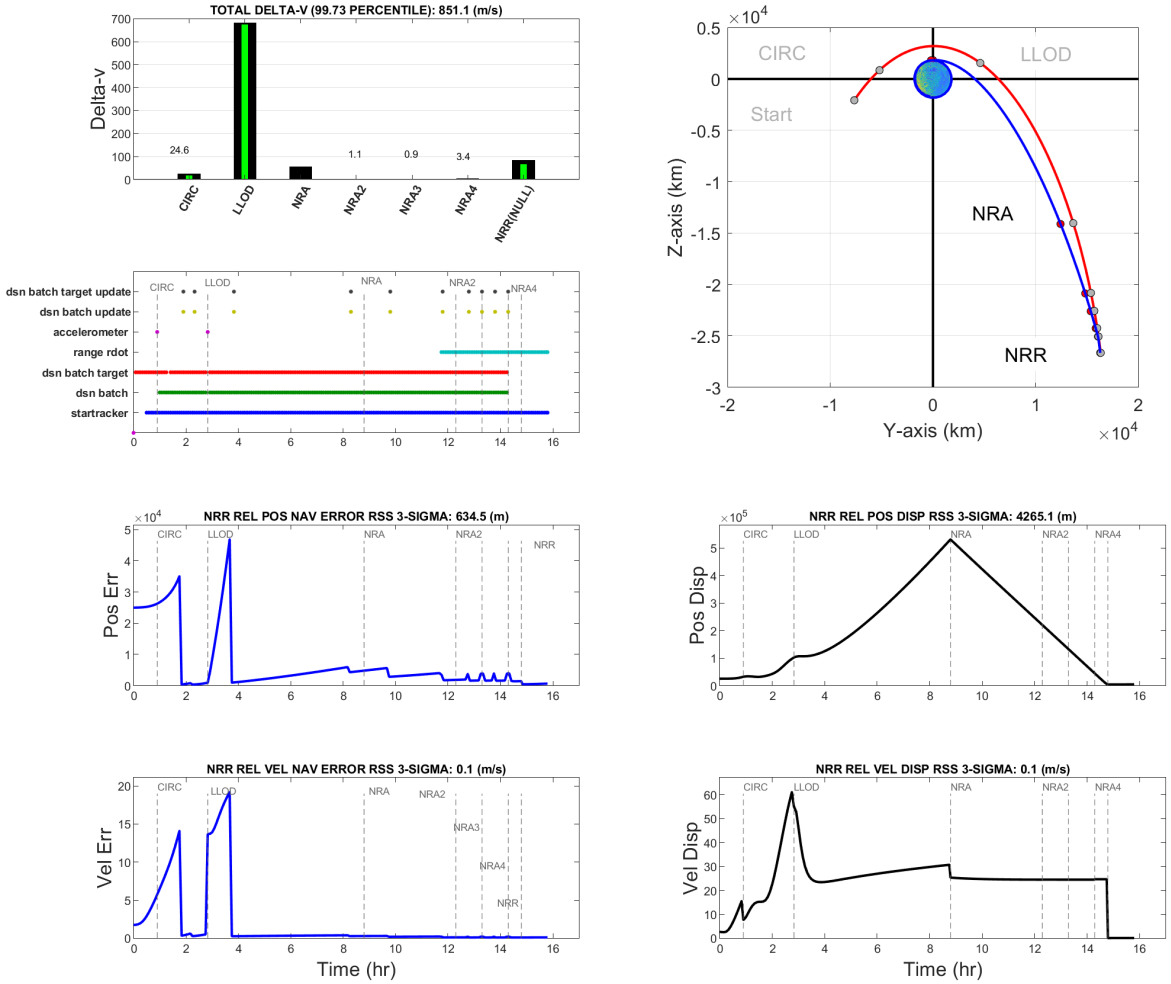

(a) Relative Trajectory Dispersions

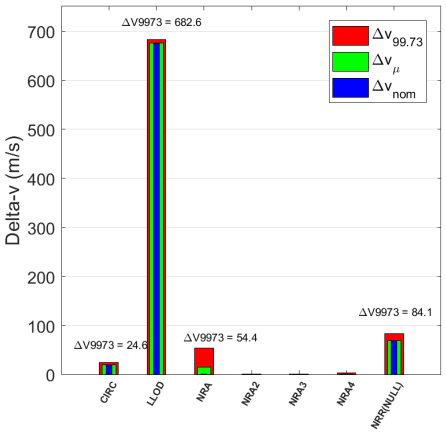

Maneuver Name	TIG (MET) (d:h:mm:ss)	ΔV_{nom} (m/s)	ΔV_{μ} (m/s)	$\Delta V_{\mu+3\sigma}$ (m/s)	ΔV_{99} (m/s)	$\Delta V_{99.73}$ (m/s)
CIRC	0:00:54:07	19.6	20.0	22.8	23.5	24.6
LLOD	0:02:49:48	675.5	675.5	683.2	681.4	682.6
NRA	0:08:47:42	0.8	15.3	46.8	46.9	54.4
NRA2	0:12:17:42	0.0	0.4	1.0	1.0	1.1
NRA3	0:13:17:42	0.0	0.3	0.8	0.8	0.9
NRA4	0:14:17:42	0.0	1.0	3.0	3.0	3.4
NRR	0:14:47:42	68.9	69.2	83.7	81.3	84.1
TOTAL	0:15:47:42	764.7	781.7	815.4	838.0	851.1

(b) Relative Navigation Errors

Figure 11. Relative Navigation Errors and Trajectory Dispersions

shown on the left and the numerical values at key epochs are shown in the table at the top right of the figure. In this instance the trajectory profiles for both HLS and Orion are reproduced in the Earth-Moon rotating frame to give geometrical context to the data. The time history plots clearly show that the navigation errors have a unique signature from the trajectory dispersions, but close examination can show how each are correlated to and impact one another. At NRR the relative 3-sigma position navigation errors are actually within 1.5 km and the relative navigation velocity 3-sigma errors are less than 0.15 m/s.

Integrated GN&C Performance Overview Lastly, to summarize all the previous results, Figure 11 brings all the previous metrics together and also includes the connection of navigation errors, trajectory dispersions, and the nominal trajectory to the resulting delta-v performance. Figure 11(a) highlights the total delta-v in the top left plot, which includes both the nominal (solid green bar) and the total 99.73 percentile delta-v (thick black bar). Below this plot is the scheduling and utilization of the different sensor measurements. The relative navigation errors in position and velocity magnitudes are available in the bottom left plots shown with solid blue lines; whereas, the resulting relative dispersions in position and velocity are provided on the bottom right plots with solid black lines. The vertical dashed lines in these plots indicate when the various translational burns occur. For reference, the HLS and Orion nominal trajectory profiles in the Earth-Moon rotating frame is included in the top right plot.

Figure 11(b) includes greater detail about the delta-v performance by providing the numerical values for the nominal, average, mean plus 3-sigma dispersed values, the delta-v 99 percentile, and the delta-v 99.73 percentile for each individual burn and total. It is worthwhile to emphasize that even though the initial NRA trajectory correction burn is nominally zero, due to uncertainty in the system, it can be as large as 56 m/s. The other correction burns (NRA2-NRA4) are much smaller, but the placement of these burns can have a noticeable influence on the total delta-v.

CONCLUSION

In conclusion, upcoming NASA Artemis missions require the complex interaction of multiple spacecraft, each utilizing and depending on data generated from multiple GN&C systems ranging from on-orbit vehicles to monitoring ground stations. Having the capability to model and capture this dependency in terms of integrated performance becomes a monumental challenge for engineers, managers, and operators. This paper has taken some initial steps to propose how linear covariance techniques can be utilized to help address these types of problems. A notional scenario relative to the Artemis III mission, where the HLS lander ascends from the lunar surface and must rendezvous with the Orion spacecraft in an NRHO reference trajectory, both motivated and started to demonstrate these proposed techniques. As human exploration initiatives and goals continue to expand and slowly become reality, there will grow an increased need to model and incorporate a multi-vehicle, multi-GN&C system arrangement to support a variety of applications, especially for rendezvous and docking phases of flight.

REFERENCES

[1] J. Williams, D. E. Lee, R. J. Whitley, K. A. Bokelmann, D. C. Davis, and C. F. Berry, "Targeting cislunar near rectilinear halo orbits for human space exploration," in *American Astronautical Society*, pp. AAS 17–267, 1017.

[2] D. J. Grebow, M. T. Ozimek, K. C. Howell, and D. C. Folta, "Multibody orbit architectures for lunar south pole coverage," *Journal of Spacecraft and Rockets*, vol. 45, no. 2, March-April 2008.

[3] D. Woffinden, "Evaluating relative navigation filter designs and architectures for human spaceflight," (Breckenridge, CO), AAS 20-042, 1 Feb - 7 Feb 2020.

[4] G. N. Holt, C. N. D'Souza, and D. Saley, "Orion optical navigation progress toward exploration mission 1," (Kissimmee, FL), AIAA 2018-1978, 8-12 January 2018.

[5] J. Orphee, M. Hannan, N. Ahmad, E. Anzalone, E. Braden, S. Craig, J. Everett, K. Miller, and N. Olson, "Guidance, navigation, and control for nasa lunar pallet lander," (Breckenridge, CO), AAS 19-033, 1 Feb - 6 Feb 2019.

[6] P. S. Maybeck, *Stochastic models, estimation, and control*, vol. 1. New York: Academic Press, 1979.

[7] D. K. Geller, "Linear covariance techniques for orbital rendezvous analysis and autonomous onboard mission planning," *Journal of Guidance, Control, and Dynamics*, vol. 29, pp. 1404–1414, November-December 2006.

[8] T. J. Moesser and D. K. Geller, "Guidance and navigation linear covariance analysis for lunar powered descent," in *AAS/AIAA Astrodynamics Specialist Conference*, (Mackinac Island, Michigan), AAS 07-313, 19-23 August 2007.

[9] D. Geller and D. Christensen, "Linear Covariance Analysis for Powered Lunar Descent and Landing," *The Journal of Spacecraft and Rockets*, vol. 46, pp. 1231–1248, Nov-Dec 2009.

[10] D. Woffinden, S. Robinson, J. Williams, and Z. Putnam, "Linear covariance analysis techniques to generate navigation and sensor requirements for the safe and precise landing - integrated capabilities evolution (splice) project," in *AIAA Scitech 2019 Forum*, (San Diego, CA), AIAA 2019-0662, 7-11 January 2019 2019.

[11] J. W. Williams, W. E. Brandenburg, D. C. Woffinden, and Z. R. Putnam, "Validation of linear covariance techniques for mars entry, descent, and landing guidance and navigaiton performance analysis," in *AIAA Scitech 2022 Forum*, 2022.

[12] R. Zanetti, D. C. Woffinden, and A. Sievers, "Multiple Event Triggers in Linear Covariance Analysis for Spacecraft Rendezvous," *Jounral of Guidance, Control, and Dynamics*, vol. 35, pp. 353–366, March-April 2012.

[13] B. G. Marchand, K. Howell, and R. Wilson, "Improved corrections process for constrained trajectory design in the n body problem," *Journal of Spacecraft and Rockets*, vol. 35, pp. 1–33, July 2007.

[14] M. W. Weeks, B. G. Marchand, C. W. smith, and S. Scarritt, "Design of the onboard autonomous targeting algorithm for the trans-earth phase of orion," (Honolulu, Hawaii), AIAA Guidance, Navigation and Control Conference and Exhibit, 18-21 August 2008.

[15] B. G. Marchand, M. W. Weeks, C. W. Smith, and S. Scarritt, "Onboard autonoous targeting for the trans-earth phase of orion," *Journal of Guidance, Control, and Dynamics*, vol. 33, pp. 943–956, May-June 2010.

[16] S. Scarritt, B. G. Marchand, A. J. Brown, W. H. Tracy, and M. W. Weeks, "Finite-burn linear targeting algorithm for autonomous path planning guidance," *Journal of Guidance, Control, and Dynamics*, vol. 35, pp. 1605–1615, September-October 2012.

[17] S. K. Scarritt, T. Fill, and S. Robinson, "Advances in orion's on-orbit guidance and targeting system architecture," (Breckenridge, CO), AAS 15-096, 1 Feb - 6 Feb 2015.

[18] B. C. Collicott and D. C. Woffinden, *Lunar Navigation Performance using the Deep Space Network and Terrain Relative Navigation to Support Precision Landing*. 19-21 January 2021.

[19] A. M. Dwyer-Cianciolo, C. D. Karlgaard, D. Woffinden, R. A. Lugo, J. Tynis, R. R. Sostaric, S. Striepe, R. Powell, and J. M. Carson, "Defining navigation requirements for future missions," in *AIAA Scitech 2019 Forum*, (San Diego), 2019. 2019-0661.